RI 9458

REPORT OF INVESTIGATIONS/1993

Behavior of Simulated Longwall Gob Material

By Deno M. Pappas and Christopher Mark

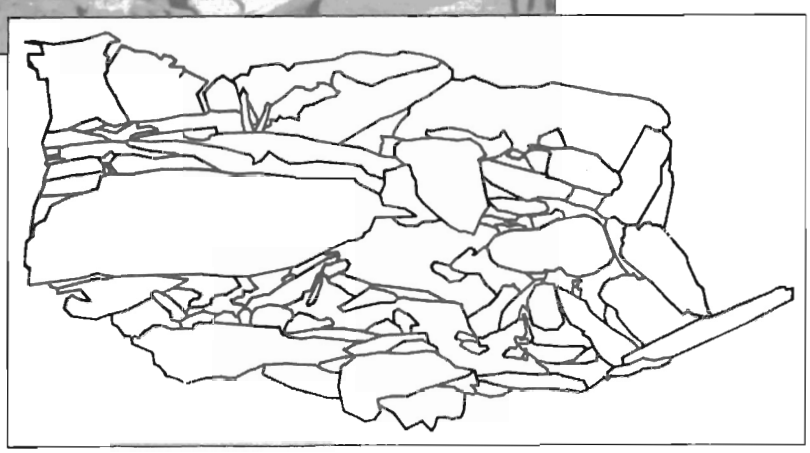

United States Department of the Interior

Bureau of Mines

Cover: Mine gob photograph (top) is digitized (bottom) to obtain approximate particle size gradation of gob material for use in laboratory studies.

Report of Investigations 9458

Behavior of Simulated Longwall Gob Material

By Deno M. Pappas and Christopher Mark

UNITED STATES DEPARTMENT OF THE INTERIOR
Bruce Babbitt, Secretary

BUREAU OF MINES

Library of Congress Cataloging in Publication Data:

Pappas, Deno M.

Behavior of simulated longwall gob material / by Deno M. Pappas and Christopher Mark.

p. cm. — (Report of investigations; 9458)

Includes bibliographical references (p. 30).

1. Coal mine waste—Mechanical properties. 2. Soil consolidation—Computer simulation. 3. Longwall mining. I. Mark, Christopher. II. Title. III. Series: Report of investigations (United States. Bureau of Mines); 9458.

TN23.U43 [TN803] 622 s—dc20 [622'.334] 92-34621 CIP

CONTENTS

ILLUSTRATIONS

ILLUSTRATIONS—Continued

TABLES

TABLES—Continued

UNIT OF MEASURE ABBREVIATIONS USED IN THIS REPORT

ft	foot	lbf	pound (force)
in	inch	lbf/ft^3	pound (force) per cubic foot
in^2	square inch	lb/ft	pound per linear foot
in^3	cubic inch	mm	millimeter
in/in	inch per inch	pct	percent
kip	1,000 pounds	psi	pound (force) per square inch
lb	pound	s	second

BEHAVIOR OF SIMULATED LONGWALL GOB MATERIAL

By Deno M. Pappas[1] and Christopher Mark[2]

ABSTRACT

This report presents results of a U.S. Bureau of Mines study of longwall gob material. The objective of this work was to determine material stiffness properties of the gob for use in numerical models of rock mass response to longwall mining. Photographs of actual mine gob were digitized to obtain approximate particle size gradations of gob material. The gradation curve was shifted down to a laboratory scale, and 20 uniaxial compression tests were conducted. Varying the maximum particle size was not found to affect the stress-strain behavior, but changing the gradation appeared to influence the stress-strain behavior. The stress-strain relationship of the simulated gob material was nonlinear, the stress-secant-modulus relationship was approximately linear, and the stress-tangent-modulus relationship was approximately a second-order polynomial function. Equations were generated from these curves, providing numerical modelers with a means to estimate gob moduli based on the stress level. In addition, the experimental data were statistically evaluated using multiple regression analyses, producing a series of equations to predict the secant and tangent moduli from the given stress level, bulking factor, rock strength, and thickness-to-width shape ratio of the particles.

[1]Research civil engineer.
[2]Mining engineer.
Pittsburgh Research Center, U.S. Bureau of Mines, Pittsburgh, PA.

INTRODUCTION

In the past 10 years, longwall productivity has broken records nearly every year. As a result, many large mining companies have begun to realize that the only way their mines can stay competitive in the domestic and world markets is to adopt longwall mining methods. With such a great interest in longwall mining, there is considerable need to know the behavior of the underground environment during the longwall mining process.

While the longwall face moves forward, the shield supports advance and the roof is allowed to cave behind the face. As the roof falls, the volume of caved material, referred to as the "gob," expands upward until it comes in contact with the sagging, fractured roof strata. Gradually the gob consolidates enough to start accepting the large loads resulting from the overburden weight. The mechanical and physical behavior of the gob material during this consolidation cycle has received little attention. This is due to the inaccessibility of the gob, which makes it difficult to study in situ. The behavior of the gob is very important in understanding the complex ground response to longwall mining, in particular for numerical modelers. With limited data, numerical modelers have in the past used estimates of gob modulus values that ranged from 1,000 psi to over 300,000 psi. Such wide variations in the moduli greatly affected the outcome of the numerical analyses, since the stiffness of the gob is a major component in the overall behavior of the model (*1*).[3]

The numerical model computer program MULSIM/NL was recently redesigned to incorporate the nonlinear stress-strain behavior of the gob that allows for strain hardening to occur (*2*). It is hypothesized that the strain-hardening behavior best models the consolidation of the gob. As the gob consolidates under increasing strain, the reduction in the void spaces makes the stress increase at an exponential rate. This implies that the slope of the gob stress-strain curve (tangent modulus) increases with increasing stress or strain. Better understanding of the behavior of the gob will allow numerical models to be more accurately applied for simulating longwall mining conditions. Also, better estimates of the gob modulus may find applications in analysis of stoping in metal and nonmetal mines, multiple-seam mine design, and surface subsidence.

The U.S. Bureau of Mines goals with this laboratory study were to estimate the gradation of actual gob material, evaluate the stress-strain behavior of simulated gob material using load deformation tests, and determine the test parameters that influence the gob modulus. The ultimate goal was to predict the gob modulus of material with specific attributes based on the test results. This work is in support of the Bureau's program to improve the safety of coal mines, through the development of predictive methods to identify potential ground control hazards.

BACKGROUND

A review of past research on the load deformation characteristics of roof fall or gob material found a wide range of moduli results, as shown in table 1. (The modulus is the slope of the stress-strain curve, which will be defined in greater detail later.) The earliest study of gob performance in the United States was reported by Rice in 1929 (*3*). He evaluated the strength of cribbing and roof debris used in anthracite mines and determined the stress-strain behavior of mine rock material under a uniaxial load. Based on Rice's results, the secant modulus value at the 800-psi stress level for confined mine rock was 2,900 psi, while confined mine rock mixed with sand and rock debris had a secant modulus of 6,600 psi (table 1). Also based on Rice's data, Peng (*4*) determined a range of secant modulus values from 1,000 psi for a loosely laid pyramidal rockpile to a maximum modulus of 47,000 psi for broken mine rock tested in a steel cylinder (table 2). The stress-strain curve was found to behave linearly for the pyramidal rockpile, but nonlinearly for the rock tested in the steel cylinder. Based on these findings, Peng (*5*) used a "rule of thumb" for estimating gob modulus. Gob modulus was estimated to range from one-hundredth to one-fifty-seventh of the intact roof rock modulus depending upon on how well the gob was packed. In 1980, Bowling (*6*) conducted a series of deformation tests at low loadings on rockfill material used for civil engineering application. Because of the low loading, the stress-strain curve was effectively linear for all of the rock types. Based on these test results, it was projected that at the 800-psi stress level the stronger rocks such as quartzite and dolerite had a secant modulus of 12,800 to 15,500 psi, whereas the weaker sedimentary rock had a modulus ranging from 5,400 to 7,200 psi, depending upon the degree of weathering (table 1).

[3]Italic numbers in parentheses refer to items in the list of references preceding the appendix at the end of this report.

Table 1.—Comparison of modulus values at a stress level of 800 psi

Reference	Year	Rock type	Modulus, psi	
			Tangent	Secant
		LABORATORY TESTS		
Rice (3)	1929	Mine rock (confined).	11,900	2,900
		Mine rock (unconfined).	12,700	2,850
		Mine rock and sand.	18,600	6,600
Bowling[1] (6)	1980	Weathered greywacke.	—	5,400
		Greywacke	—	7,200
		Dolerite	—	12,800
		Quartzite	—	15,500
DRC[2]	1990	Shale	10,100	3,200
		Sandstone	10,400	4,300
		IN SITU TESTS		
Wardle (7)	1983	Caved waste material.	—	3,100
Smart (8)	1987	..do.	7,900	3,000
Trueman[3] (9)	1990	..do.	10,150	3,000

[1]Used non-coal-measure rocks.
[2]Bureau's Denver Research Center.
[3]Added correction factor to Smart's results.

NOTE.—Dashes indicate tangent modulus result was not applicable since the stress-strain curves were linear.

Table 2.—Range of modulus values used in numerical modeling

Reference	Year	Modulus, psi	
		Tangent	Secant
Peng (4)	1978	—	[1]1,000- 47,000
Peng (5)	1978	—	[1]13,900-139,000
Hsiung (10):			
Sandstone	1985	—	[2]50,000- 87,000
Shale	1985	—	[2]20,000- 35,000
Hackett (13)	1987	—	[2]3,600-357,000
Kripakov (11)	1988	—	20,000
Park (15)	1989	—	[3]2,500- 20,000
Maleki (14)	1990	158,000	[4]13,200
Su (16)	1991	[5]1,050- 42,000	3,420
Heasley (17)	1991	—	[6]7,500

[1]Based on Rice's test results (3).
[2]Based on percent of modulus of intact rock.
[3]Based on location in gob with regard to face.
[4]Certain amount of preclosure was allowed before load transfer occurred.
[5]Low initial modulus at 22-pct compaction.
[6]Gob modulus selected for room-and-pillar retreat mining application.

NOTE.—Dashes indicate linear approximations where the tangent modulus cannot be determined.

An examination of British and Australian in-mine tests of roof fall material revealed some rather startling differences in the gob modulus from the results estimated in the laboratory findings. In 1983, Wardle (7) conducted in situ tests of caved waste piles resulting from roof failures in an Australian coal mine. The tests used hydraulic jacks to apply the load and a displacement transducer to monitor strain. Test results produced approximately linear behavior of the stress-strain curve, with an estimated deformation modulus of 3,100 psi at a maximum stress level of 200 psi. Meanwhile in the United Kingdom, Smart (8) evaluated the stress-strain behavior of a stone-built pillar, using a flatjack to apply the load to the pillar and a convergence strut to monitor displacement. Stress-strain results show a nonlinear, fourth-order polynomial curve with a secant modulus of about 3,000 psi at a vertical pressure of 800 psi. Trueman (9) modified Smart's stress-strain curve to take into account ultimate compaction of the material. This modification changed the shape of the stress-strain curve beyond 25 pct compaction because of strain hardening. With this revised equation for the stress-strain curve of a material, the secant modulus remains about the same but the tangent modulus is considerably higher.

A review of the gob moduli used in numerical model studies found an even wider range of values, as shown in table 2 (all of these values are based on a linear behavior of the gob except as noted). In determining the gob secant modulus for use in a finite-element model of a longwall panel, Peng (5) estimated that the gob moduli ranged from 13,900 psi for loosely packed gob to 139,000 psi for partially failed gob. Using Peng's rule of thumb for estimating the gob modulus, Hsiung (10) determined the gob moduli for two different rock types: sandstone ranged from 50,000 to 87,000 psi, and shale ranged from 20,000 to 35,000 psi, depending upon the gob void ratio. Within these same ranges, Kripakov (11) and Beckett (12) used a gob modulus of 20,000 psi to analyze the stress transfer around longwall panel gob zones using the computer program MULSIM/BM. Hackett (13) modified Peng's rule of thumb by widening the range of the gob modulus to 0.1, 5, and 10 pct of the intact rock modulus. Hackett used the gob modulus values of 3,600, 178,000, and 357,000 psi to model stresses in the rock interburden of a multislice longwall panel using the ADINA finite-element program. Modeling results were mixed, so that a definite gob modulus could not be pinpointed. Maleki (14) chose a model of the gob using an equivalent elastic gob tangent modulus of 158,000 psi with a certain preclosure allowed before load transfer could occur, resulting in the bilinear behavior of the gob. This approach produced a projected secant modulus of approximately 13,200 psi at the 800-psi

stress level. To account for increasing amount of compaction in the direction away from the face, Park (*15*) implemented a linear gob model ranging from 2,500 to 20,000 psi depending upon the location. Most recently, Su (*16*) chose a very low initial tangent modulus of 1,050 psi, with a higher modulus of 42,000 psi occurring after a gob compaction of 22 pct, resulting in the bilinear behavior of the gob. At the 800-psi stress level, this would result in a gob secant modulus of 3,420 psi. All of the above gob moduli values were used for modeling longwall situations; for comparison purposes, a linear gob modulus value of 7,500 psi was used by Heasley (*17*) to model pillar retreat mining.

The wide range of reported gob moduli values makes it imperative that a more accurate and uniform method of determining moduli values be established.

GOB MATERIAL SIMULATION

The first task in the laboratory tests was to develop test materials that had properties similar to those of actual gob material. The characteristics that were considered included the tensile and compressive rock strengths, rock density, surface roughness, rock shape, rock size, and size gradation. Most of these characteristics would be simulated by broken rock obtained from fresh roof falls. However, the rock size and gradation needed to be reduced to a laboratory scale.

SCALED-DOWN GRADATION CURVE

Several articles have been written evaluating scaled-down gradation curves for determining the stress-strain properties of granular materials. Marachi (*18*), Becker (*19*), and Fumagalli (*20*) determined that the grain size distribution curves for actual dam rockfill materials could be proportionally scaled down and accurately represented for laboratory tests. Marachi provides some theoretical justification with the observation that with the regular packing of ideal spheres, the strain and maximum contact stresses are independent of the particle size. In fact, his tests found that the difference in strength characteristics for 2- and 6-in maximum particle size gradations was so small that for all practical purposes, the strength and deformation characteristics of the 2-in maximum particle size materials could be considered the same as those of the larger particles. Marachi proceeds to describe a method developed by Lowe (*21*) to model samples from a prototype material. The gradation curve of the modeled material was determined by shifting the gradation curve of the prototype material, parallel to itself, to the desired maximum particle size for the laboratory sample.

GRADATION OF GOB MATERIAL

Before Lowe's method could be used to determine the gradation curve of the laboratory sample, an approximate gradation curve of actual gob material needed to be established. It has been documented that grain size distribution curves of rock blast fragments can be estimated from digitized photographs using photoanalysis software (*22*). Although photoanalysis software was not used in the current study, the basic photoanalysis techniques were applied to photographs of gob material. Photographs were taken of several longwall gob sites from the headgate entries where portions of the gob could be viewed through the crosscuts. One site was photographed in a Virginia mine in the Pocahontas Coalbed (fig. 1), and two sites were photographed in an eastern Kentucky mine in the Harlan Coalbed (figs. 2-3). Only photographs with excellent clarity and lighting can be analyzed. The basic photoanalysis technique involves tracing the outline of the photographed gob pieces (fig. 4), using a scale in the photograph to estimate the size of the rock and the frequency so that a histogram can be compiled, as shown in figure 5. When the approximate maximum diameter of the rock is known, the spherical volume of the rock can be estimated for each rock size grouping. Multiplying the total number of rock pieces by the estimated volume for each size grouping produces the total volume of rock for each size grouping. The total volume is then multiplied by the rock density to generate the weight of the rock for each size grouping. Plotting the rock size versus the percent passing (i.e., percentage of rock by weight passing a particular sieve size) generates the gradation curve of the gob rock. Figure 6 shows the estimated gradation curves for each gob site photographed and indicates that the gob gradation for these three sites may fall within a fairly narrow range. The roof rock at both mines was relatively strong, so the actual range of size distribution across the complete spectrum of U.S. longwalls may be considerably greater than is indicated by figure 6. Next, the gradation curves were corrected to account for rock pieces hidden because of the two-dimensional effect of the photograph.

The correction factor for the hidden rock was derived as follows. Mine rock material, with a known gradation curve, was piled and photographs were taken of the sides. The resulting photographs were digitized, the rock was sized, and the volumes were estimated just as they were for the actual gob photographs. The gradation curves determined from the photoanalysis were then compared with the known gradation curve. Figure 7 shows that photoanalysis seemed to accurately estimate the actual gradation curve of the rock material with the exception of the smaller particle sizes, which it underestimates.

Figure 1.—Gob of a Virginia coal mine.

Figure 2.—Gob of an eastern Kentucky coal mine—site 1.

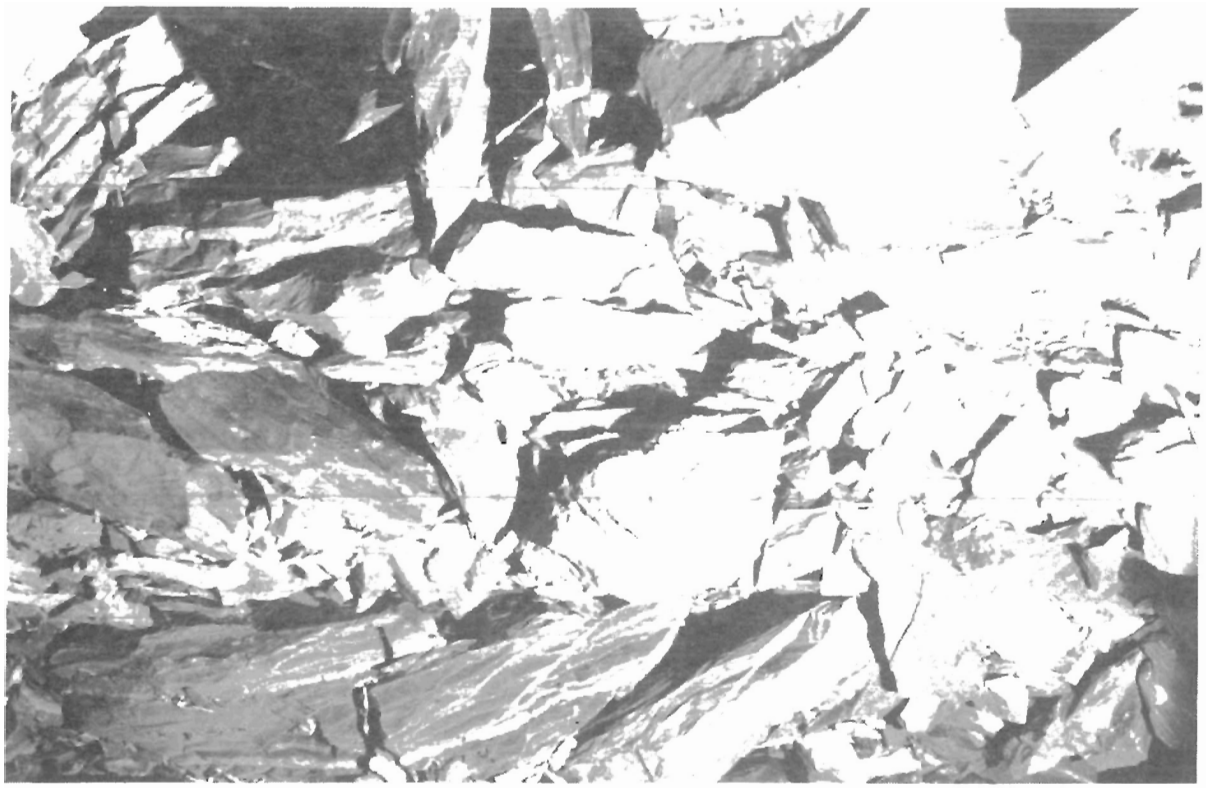

Figure 3.—Gob of an eastern Kentucky coal mine—site 2.

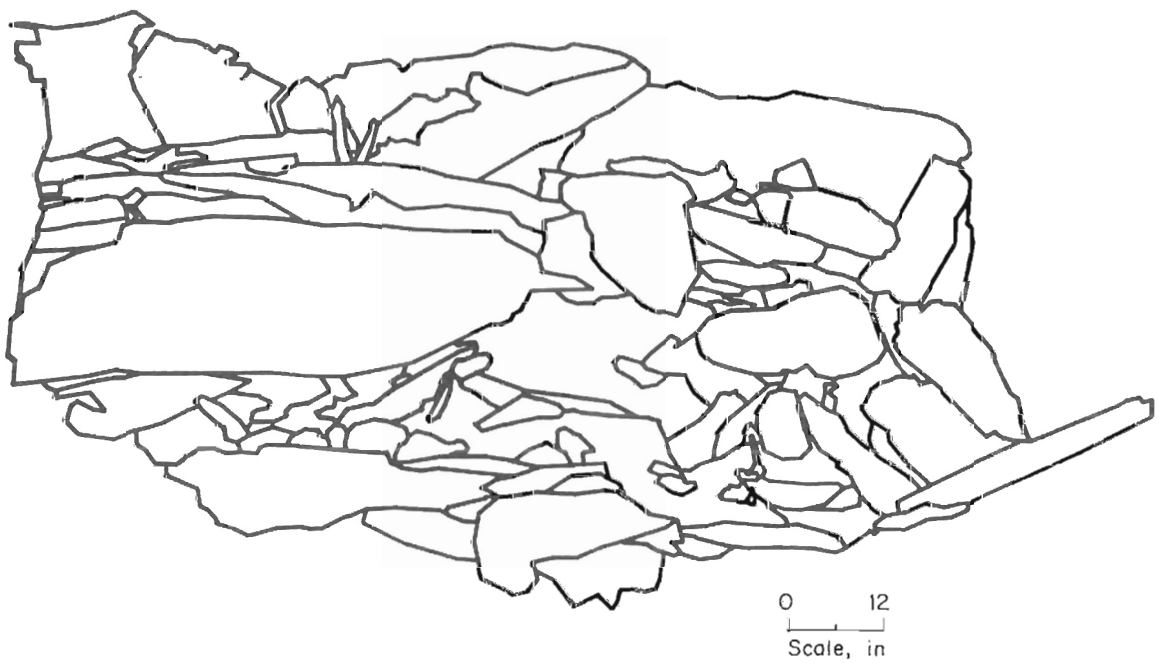

Figure 4.—Sample digitized gob based on Virginia coal mine photograph.

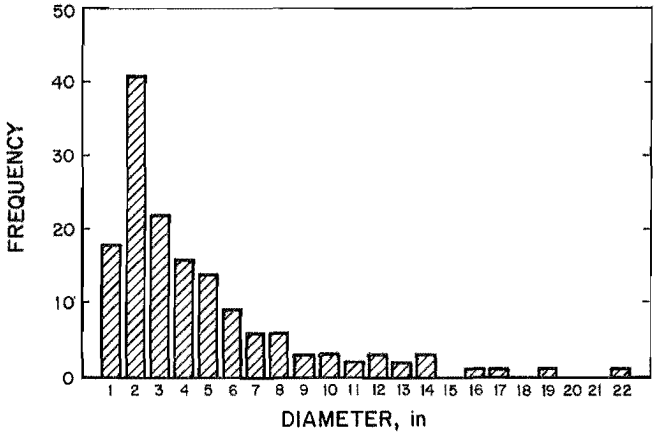

Figure 5.—Sample histogram of rock size distribution based on photoanalysis of Virginia coal mine.

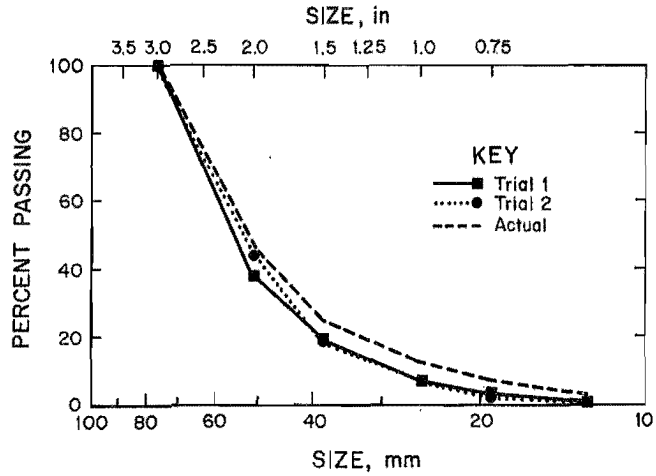

Figure 7.—Comparison of photoanalysis of laboratory rock gradation with actual gradation of laboratory rock.

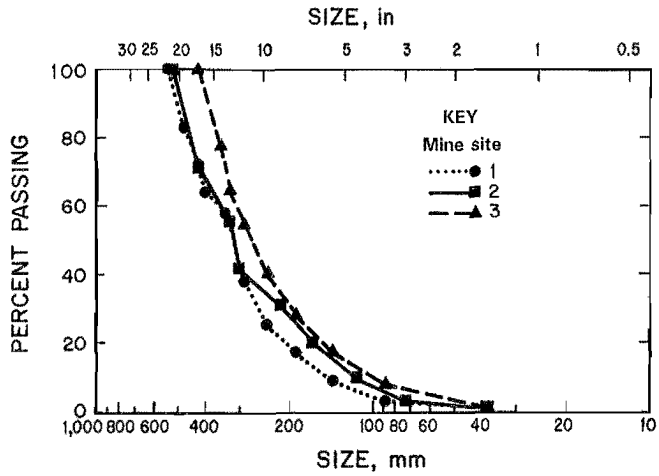

Figure 6.—Estimated gob gradation of three mine sites based on photoanalysis.

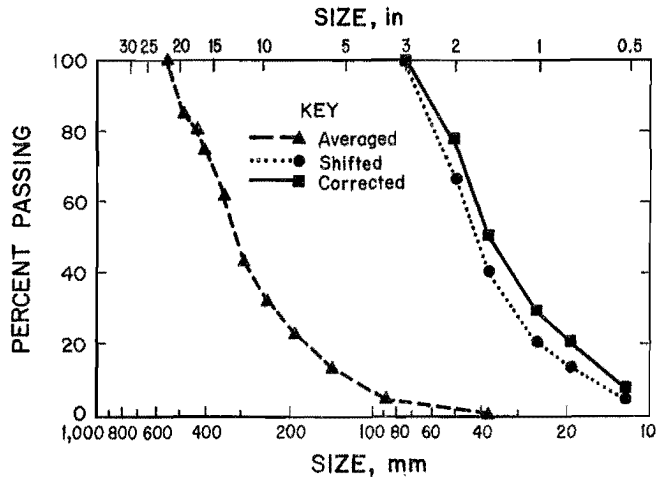

Figure 8.—Average gradation curve—mean gradation curve determined from photoanalysis of three mine sites. Shifted curve is averaged gradation curve shifted down for laboratory tests. Corrected curve is shifted gradation curve adjusted to account for hidden rock pieces.

The gradation curve for the laboratory gob material was derived by the following procedure. First, the curves in figure 6 were averaged to obtain the "averaged curve" in figure 8. The averaged curve was then shifted on the graph parallel to itself down to a maximum particle size of 3 in ("shifted curve" of figure 8). Lastly, the shifted curve of figure 8 was corrected to account for the hidden rock material in proportion to the adjustment factor determined previously. This process resulted in the "corrected curve" of figure 8, which is the simulated gradation curve of longwall gob from these three mine sites.

Once the standard test gradation curve was obtained, other curves were developed using various maximum particle sizes. Since the diameter of the test chamber is 14 in, and it has been determined that the maximum rock piece should not be more than one-third the diameter of the chamber (*23*), a maximum particle size of 3.5 in was chosen to be tested with the modeled gob gradation curve (fig. 9). The curve was also shifted parallel to maximum rock sizes of 3 in and 2 in to determine if there was any size effect in these tests (fig. 9).

SOURCE MATERIAL

Three types of rock were obtained for testing. Shale and strong sandstone were obtained from underground coal mines where these test rocks were major components in the gob of each mine's longwall system. The third rock, a weak sandstone, was obtained from a stone quarry.

These three rock types were chosen to represent the range of potential gob materials. The rocks were broken up and sorted using the following sieve sizes (inches): 3.5, 3.0, 2.5, 2.0, 1.5, 1.25, 1.0, and 0.75.

The physical characteristics of the source materials were determined using a number of different methods. The rock was evaluated based on its appearance, following the classification method of Ferm (*24*). Overall shape of the rock was evaluated using Zingg's method (as described in references *25-26*), which classifies the rock shape based on ratios of its dimensions and is discussed in detail in the section "Rock Shape." Density of the rock was determined by specific gravity tests following the ASTM guidelines (*27*). Compressive strength of the rock was estimated by a series of point load tests. The point load test compresses a piece of rock between two points using two cone-shaped platens. An irregular rock piece is compressed to failure under a point load. From the test results, a point load index is calculated and standardized by conversion to a value equivalent to results of testing a 50-mm rock core. The standardized index is averaged, excluding the two lowest and two highest values. The average index value is converted to compressive strength by using a conversion factor that was recently found by Vallejo (*28*) to be dependent upon the rock type (i.e., for shales the conversion factor is 12.5 times the averaged index value while for sandstone it is 17.4). Results of the point load tests are listed in the appendix (tables A-1—A-3).

Shale

The shale was obtained from a major roof fall in a southwestern Pennsylvania coal mine located in the Pittsburgh Coal Seam. The rock originated between 2.5 and 13 ft above the coal seam. It consisted of dark gray shale (Ferm No. 124), dark gray shale with sandstone streaks (Ferm No. 323), and black shale with coal streaks (Ferm No. 113). From point load test results, the average compressive strength was estimated to be 5,400 psi parallel to bedding and 10,500 psi perpendicular to bedding. The shale pieces broke typically into disk shapes with feathered edges, with an average density of 162.1 lbf/ft^3.

Weak Sandstone

Fresh sandstone was acquired from a southwestern Pennsylvania stone quarry. The rock occurred approximately 100 ft above the Pittsburgh Coal Seam. The rock is characterized as a medium-grained, friable, gray massive sandstone (Ferm No. 544). Point load test results estimated an average compressive strength of 6,300 psi parallel to bedding and 6,200 psi perpendicular to bedding. The sandstone pieces broke into spherical-disk shapes with less sharp edges than the shale had. Density of the sandstone was 157.5 lbf/ft^3.

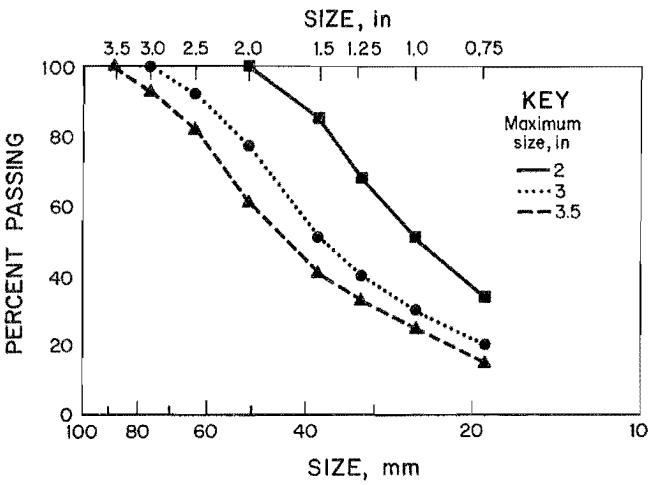

Figure 9.—Three gradation curves for laboratory tests with maximum particle sizes of 3.5, 3.0, and 2.0 in.

Strong Sandstone[4]

Although similar in appearance to the weak sandstone, the strong sandstone had a compressive strength over three times as great. Estimated point load results indicated an average compressive strength of 14,200 psi parallel to bedding and 18,300 psi perpendicular to bedding. The rock was obtained by scaling portions of the roof of a coal mine in southern West Virginia. The strong sandstone had a density of 168.4 lbf/ft^3. The rock broke into cubic pieces with well-defined edges. The massive sandstone (Ferm No. 564) was located directly above the Pocahontas No. 3 Seam and ranged in thickness from 10 to 60 ft.

[4]The authors thank Craig S. Compton, mining engineer technician, Pittsburgh Research Center, for his diligent efforts in obtaining the strong sandstone test material from an underground mine.

LOAD DEFORMATION TEST

Because there are no published standards for conducting load deformation tests of granular material, and since several different methods have been employed (as described in the literature), the apparatus, procedures, methodology, and analysis techniques required for these tests were developed.

TEST APPARATUS

The apparatus used for the load deformation tests is composed of two parts, the chamber and the platen (fig. 10). The steel chamber is made out of 16-in-OD (14.31-in-ID) by 12-in ASA 80 pipe with a thickness of 0.843 in; it is bolted and welded to a 20- by 20- by 1-in base. The chamber has a removable quarter section that is fastened to the stationary part of the chamber with five bolts on either side (figs. 10-11). The exterior walls of the test chamber are instrumented with strain gauges to monitor horizontal and vertical movements.

The upper platen component consists of 14.16-in-diameter by 2-in-thick steel plate. A 9.5-in-diameter by 5-in-thick spacer is also used to maximize the available stroke of the test machine. The clearance between the platen and the inside walls of the chamber is about 0.08 in.

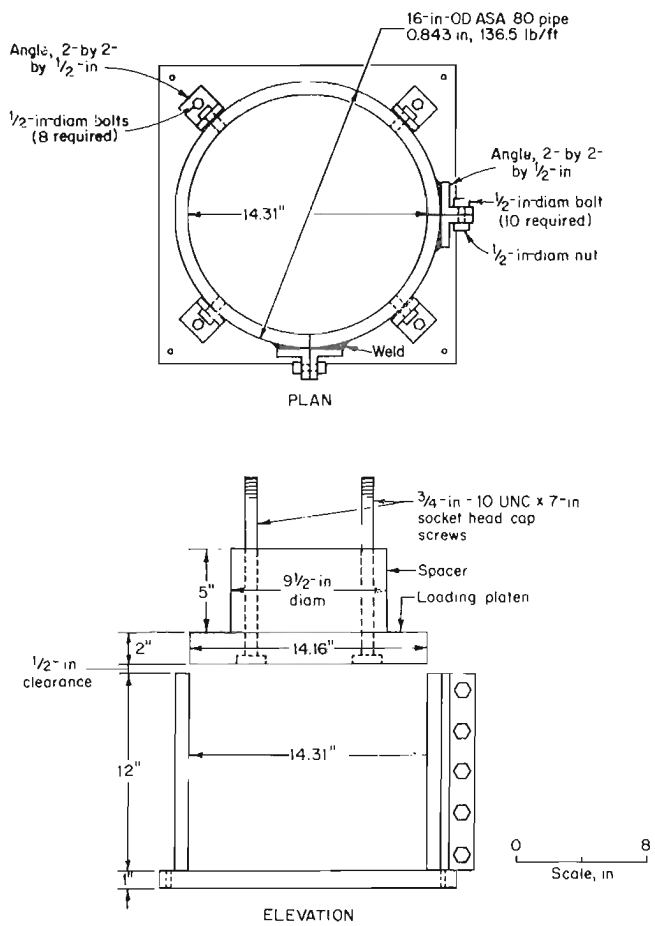

Figure 10.—Plan and elevation views of test chamber and platens.

TEST PROCEDURE[5]

To begin each test, the size-sorted rock is weighed out according to the proportions indicated by the simulated gob gradation curves determined previously. Rock from each size grouping is sampled and measured (length, width, and thickness) to evaluate shape effect. The rock is then thoroughly mixed together in a trough to ensure uniform composition.

The simulated gob for the laboratory tests is shoveled into the test chamber until it reaches about an inch below the lip of the chamber top (fig. 11). The weight of the rock in the test chamber is determined by subtracting the weight of the gob material remaining in the trough after filling the chamber from the weight of the original

[5]The authors thank Michael DiMartino, electronics technician, Pittsburgh Research Center, for his input and assistance in conducting the load deformation tests.

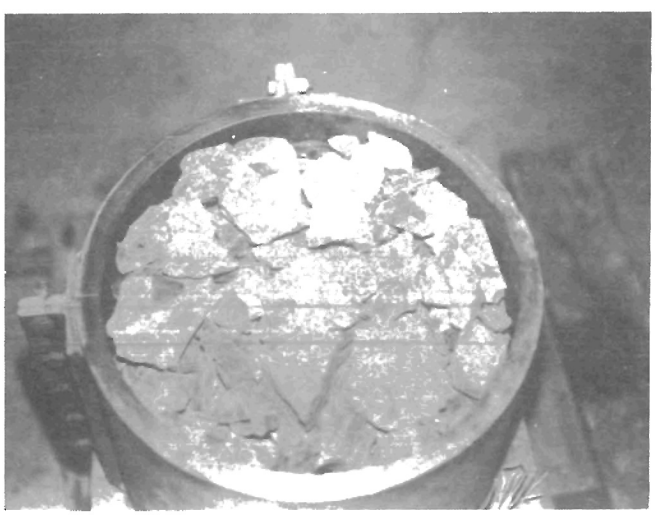

Figure 11.—Simulated gob in test chamber.

material. The weight of the rock in the chamber is needed to determine the void ratio. Placed on top of the rock is a layer of cellophane film and moist, uniformly graded sand. The sand is compacted and leveled with the top of the chamber (fig. 12). The purpose of the sand is to ensure a smooth testing surface so that load application of the upper platen is uniformly distributed, while the cellophane film minimizes sand infiltration into the simulated gob material.

The filled test chamber is moved by forklift into the laboratory and placed into the 1-million-lb load frame (fig. 13). Finally, the top loading surface of the chamber is aligned with the top of the testing machine's upper platen.

Since the vertical displacement of the material exceeds the stroke of the testing machine, the tests are conducted in two parts. After 2 in of displacement, the test machine's platens are extended, and the test continues for 3 additional inches or until the load reaches 500,000 lb. Additional stroke for the second phase of the test is obtained by attaching rods between the base of the chamber and angle irons placed over the top of the testing machine. The load on the chamber base is then released, and a 2-in-thick spacer is placed beneath the suspended chamber. Finally, the loading platen with the spacer is moved up against the chamber base, and the test is restarted.

A 458.20 MTS MicroConsole[6] unit is used to control the MTS 1,000-kip servocontrolled testing machine (fig. 13). Initially, the load controller is set to a zero reading. A light preload (<1 pct) is applied to the loading surface of the simulated gob material to zero the displacement LVDT (linear variable differential transformer) within the load cell. Load is then applied at a preset ramp rate using a specially designed program created on the 458.91 Microprofiler control unit. The program is set to provide the desired ramping rate on the test material until a maximum load of 500 kips is reached or the stroke of the LVDT is exceeded. A Micromac 4,000 data acquisition system is used to monitor load, displacement, and chamber strains. Readings are taken at 4-s intervals, with data stored on a personal computer. Raw data are later transferred to a Vax mainframe computer for data reduction and analysis using the RS/1 software package.

Upon completion of the load deformation test, the chamber is removed from the testing machine and the quarter panel of the chamber is detached. Figure 14 shows that the simulated gob material compresses about 3.5 to 4 in after a maximum load of 500,000 lbf. The test remains are sieved to determine particle breakage, and various sizes of rock pieces are sampled and measured to determine changes in particle shape.

[6]Reference to specific equipment does not imply endorsement by the U.S. Bureau of Mines.

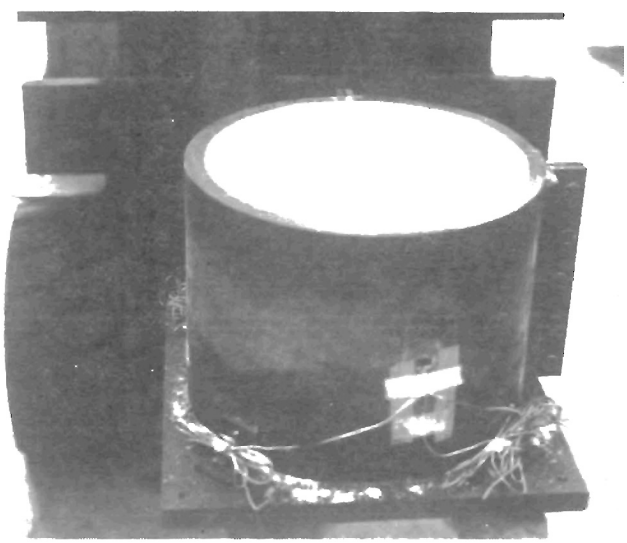

Figure 12.—Test chamber filled with simulated gob and topped with layer of sand.

TEST METHODOLOGY

The goal of the laboratory tests was to determine how maximum particle size, particle shape, particle breakage, void ratio, and rock strength affect the stress-strain behavior (i.e., the secant and tangent moduli) of the simulated gob material. The ultimate goal of the tests was to develop an equation for predicting the moduli.

Table 3 shows the individual tests that were run and the parameters that were varied. Each rock type varied in overall particle shape and strength (see "Source Material," which defines these characteristics for each rock type). Maximum size of the test material ranged from 2 to 3.5 in. The gradation curve used for the test material was the curve shown in figure 9, except that one test used a uniform-size rock. The maximum load applied to the simulated gob material increased as the test series progressed and as additional stroke capability of the test machine was made available.

ANALYSIS TECHNIQUES

The data from the load deformation tests were analyzed to determine several parameters, as summarized below and in table 4. Some of these parameters were evaluated at the initiation and conclusion of the test (zero and maximum load of the test) and/or at a stress level of 800 psi. The stress level of 800 psi represents 730 ft of overburden, which is typical of many U.S. longwalls.

Percent Compaction

The amount of strain (ϵ) or percent compaction of the simulated gob material is defined as follows:

$$\epsilon = \frac{D}{H}, \qquad (1)$$

where D = cumulative displacement of rock material, in,

and H = initial height of test material, in.

Although these values are dependent upon the maximum load applied, the percent compaction does give an indication of the compressibility of the rock type when evaluated at equivalent maximum loadings. During some of the tests, the axial strain was monitored during the unloading of the test material to evaluate the rebound of the rock. The type of strain shown in equation 1 is known as the engineering strain and not the true strain, which corrects the initial height for each increment of displacement.

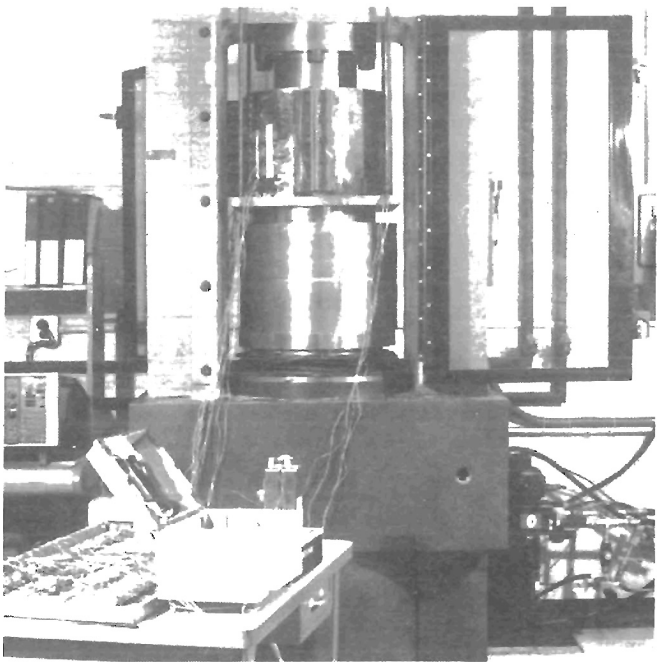

Figure 13.—Load deformation test setup.

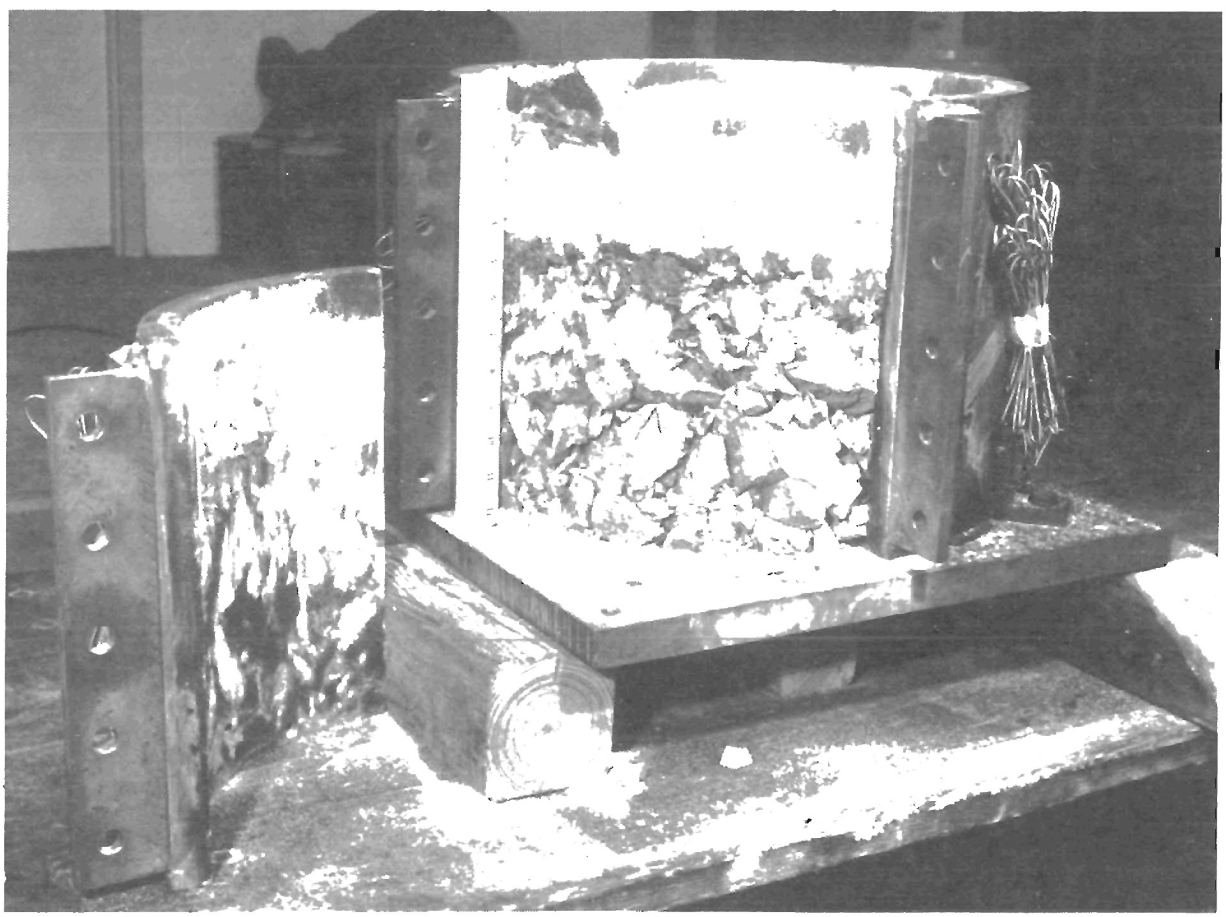

Figure 14.—Simulated gob material following completion of test.

Table 3.—Load deformation test series and parameters varied

Test	1	2	3	4	5	6	7	8	9	10
Rock type:										
Shale	X	X	X	X	X	X	X	X	X	X
Weak sandstone										
Strong sandstone										
Maximum size:										
2 in				X		[1]			X	
3 in	X	X	X				X	X		
3.5 in					X					X
Gradation:										
Standard[2]	X	X	X	X	X		X	X	X	X
1 size						X				
Layered								X		
Maximum loading:										
700 psi	X	X	X	X	X					
1,300 psi						X	X	X		
3,000 psi									X	X
6,000 psi										

	11	12	13	14	15	16	17	18	19	20
Rock type:										
Shale						X	X			
Weak sandstone	X	X	X	X	X					
Strong sandstone								X	X	X
Maximum size:										
2 in				X						
3 in	X	X	X			X	X	X	X	X
3.5 in					X					
Gradation:										
Standard[2]	X	X	X	X	X	X	X	X	X	X
1 size										
Layered										
Maximum loading:										
700 psi										
1,300 psi										
3,000 psi	X	X	X	X	X		X	X	X	X
6,000 psi						X				

[1]Maximum size, 2.5 in.
[2]See figure 9.

NOTE.—X indicates parameter used in test.

Void Ratio

Indirectly determined is the void ratio, which indicates the amount of void space present in the test material. As the void ratio decreases, the material is more densely compacted. The void ratio can be determined by using the rock density, amount of rock in the test chamber, and cumulative deformation of the simulated gob material. The formula is somewhat complicated by the layer of sand on top of the simulated rock material. First, the average height of the sand layer is determined by dividing the sand's weight by its density, and dividing by the inside area of the chamber.

$$H_s = \frac{W_s}{\gamma_s} \times \frac{1728}{A}, \qquad (2)$$

where H_s = layered sand height, in,

W_s = layered sand weight, lbf,

γ_s = density of the sand, lbf/ft^3,

and A = inside area of test chamber, in^2.

Table 4.—Summary of load deformation test results

Test	Maximum size, in	Maximum stress, psi	Compaction, pct	Void ratio[1]			Bulking factor[2]	Modulus,[2] psi		Particle breakage
				v_0	v^{800}	v_f		Secant	Tangent	
1	3	700	25.8	0.887	—	0.406	—	—	—	135.8
2	3	760	27.1	.788	—	.310	—	—	—	120.7
3	3	740	28.3	.831	—	.320	—	—	—	150.4
4	2	750	28.4	.908	—	.373	—	—	—	89.8
5	3.5	530	29.6	.840	—	.303	—	—	—	122.2
6	[3]2.5	1,230	41.8	.831	0.139	.078	1.14	2,073	9,933	356.3
7	3	1,250	35.3	.855	.280	.210	1.28	2,547	8,921	158.4
8	3	1,260	36.5	.852	.253	.185	1.25	2,428	9,290	186.0
9	2	2,790	36.1	.802	.365	.160	1.36	3,258	7,560	126.4
10	3.5	3,130	36.3	.679	.269	.078	1.27	3,231	8,587	242.2
16	3	6,083	43.9	.765	.308	.002	1.31	3,025	7,839	242.5
17	3	2,820	37.9	.787	.312	.128	1.31	2,917	8,309	182.2
WEAK SANDSTONE										
11	3	3,120	33.1	0.701	0.311	0.147	1.31	3,494	8,703	180.1
12	3	3,150	35.2	.779	.343	.163	1.34	3,200	8,820	187.3
13	3	3,150	34.1	.724	.312	.144	1.31	3,281	9,698	168.5
14	2	2,840	36.2	.790	.313	.152	1.31	2,924	8,584	88.7
15	3.5	3,110	32.9	.719	.337	.162	1.34	3,573	9,331	193.4
STRONG SANDSTONE										
18	3	3,130	34.8	0.866	0.471	0.249	1.47	3,569	7,251	117.2
19	3	3,160	31.2	.878	.495	.260	1.49	3,829	8,208	132.9
20	3	3,160	33.7	.856	.497	.248	1.50	4,295	8,826	133.2

[1] v_0, at zero load; v_{800}, at 800 psi; v_f, at final load.
[2] At 800 psi.
[3] Only 1 particle size used.

NOTE.—Dashes indicate data unavailable because of low stress level of test.

During the test, some sand squeezes out around the loading platen and sticks uniformly along the circumference of the chamber walls. This factor can be accounted for by determining the weight of sand sticking to the chamber walls (per inch of displacement) and subtracting the weight of the wall sand from the layered sand.

$$H_s = \frac{W_s - W_{sc}}{\gamma_s} \times \frac{1728}{A}, \qquad (3)$$

where W_{sc} = sand weight on chamber walls, lbf.

Subtracting the average height of the layered sand, minus the amount of cumulative displacement, from the original height of the chamber (12 in) results in the true rock material height at that particular point in time during the test.

$$H_r = H_c - H_s - D, \qquad (4)$$

where H_r = height of test rock material, in,

H_c = height of test chamber, in,

H_s = height of layered sand, in,

and D = cumulative displacement, in.

Multiplying the height of the test material by the area of the chamber produces the total volume (V_t) occupied by the test material (including voids) at that point in time.

$$V_t = H_r \times A. \qquad (5)$$

The volume of the rock material (V_r) can be determined as

$$V_r = \frac{W_r}{\gamma_r} \times 1728, \qquad (6)$$

where W_r = weight of test rock material, lbf,

and γ_r = density of test rock material, lbf/ft^3.

The void ratio can be determined:

$$e = \frac{V_v}{V_r}, \quad (7)$$

$$V_v = V_t - V_r, \quad (8)$$

$$e = \frac{(V_t - V_r)}{V_r}, \quad (9)$$

where e = void ratio,

V_v = void volume, in^3,

V_r = test material volume, in^3,

and V_t = total volume, in^3.

The void ratio was determined for each point of displacement using a spreadsheet software program. In addition, the "bulking factor" (BF) may be determined as the ratio of the total volume of the broken rock material (including voids) divided by the volume occupied by the intact rock, or the void ratio plus 1:

$$BF = \frac{V_t}{V_r}, \quad (10)$$

or

$$BF = \frac{(V_t - V_r)}{V_r} + \frac{V_r}{V_r}, \quad (11)$$

$$BF = e + 1. \quad (12)$$

The bulking factor is often used in the literature to determine the height of the caving zone (*29*). Table 4 lists the bulking factor at the 800-psi stress level.

Particle Breakage

After the test, the rock material was sieved and the grain size distribution curve was compared with the pretest gradation curve. Overall particle breakage was quantified by subtracting the amount of rock particles passing each sieve before the test from the amount of rock passing after the test and summing the negative difference according to the method used by Marsal (*30*). The appendix lists all of the pretest and posttest grain size distribution curves (fig. A-1).

Rock Shape

Zingg's classification method (*25-26*) was used to quantify the shape of the rock pieces before and after each test, as well as to compare shapes of the three different rock types. For each test, at least eight rocks were sampled from each sieve size, and the length, width, and thickness of the rock pieces were measured. The ratio of the thickness to width is plotted on the x-axis, while the ratio of the width to length is plotted on the y-axis. Figure 15 shows the various classifications by shape (spheroid, blade, roller, and disk) and the classification of each rock type before and after the tests.

Contact Points

To evaluate how well the various rock types are able to transmit an applied load through the skeletal structure of the granular material, the number of contacts per particle was determined according to the method used by Athanasiou-Grivas (*31*). The number of contact points was determined by randomly placing test rock material of a specific gradation into an aquarium equal to the test chamber in size, shape, and cross-sectional area (160 in^2). The aquarium was then filled with white paint, which was allowed to drain freely from the bottom and was left to dry. The points of contact between particles were distinguishable by unpainted portions on the rocks or white splotches due to capillary concentrations of the paint where the rocks were in contact (fig. 16). Approximately 300 rocks were sampled at various levels, and the number of contact points was counted and averaged. This procedure was repeated for each rock type using the same gradation and quantity of simulated gob material.

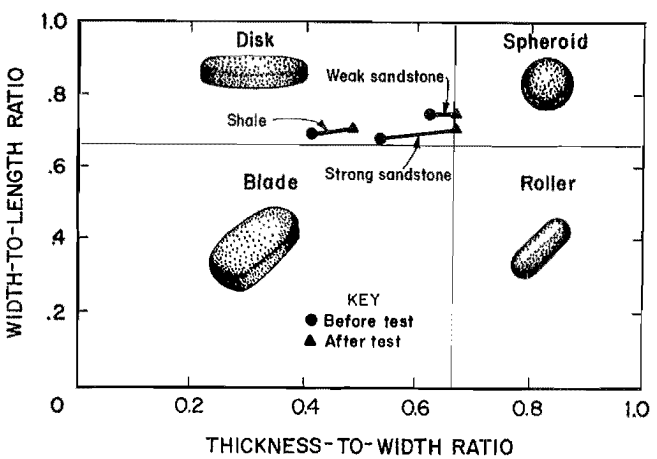

Figure 15.—Shape classification chart (25-26).

Secant and Tangent Moduli

The direct results obtained from these tests are the load and displacement readings, from which the vertical stress and strain are determined as follows:

$$\sigma = \frac{L}{\pi r^2}, \quad (13)$$

$$\epsilon = \frac{D}{H}, \quad (14)$$

where σ = vertical stress, psi,

L = applied load, lbf,

r = radius of platen applying load, in,

ϵ = strain, in/in,

D = cumulative displacement of rock material, in,

and H = initial height of test material, in.

Indirectly from these stress and strain values can be determined two types of moduli of the simulated gob material, which give an indication of the stiffness of the material. Both moduli are obtained from the slope of the stress-strain curve; the secant modulus is the slope of a line from a point in question on the stress-strain curve to the origin, while the tangent modulus is the slope of a line tangent to that point (fig. 17). The moduli are expressed as follows:

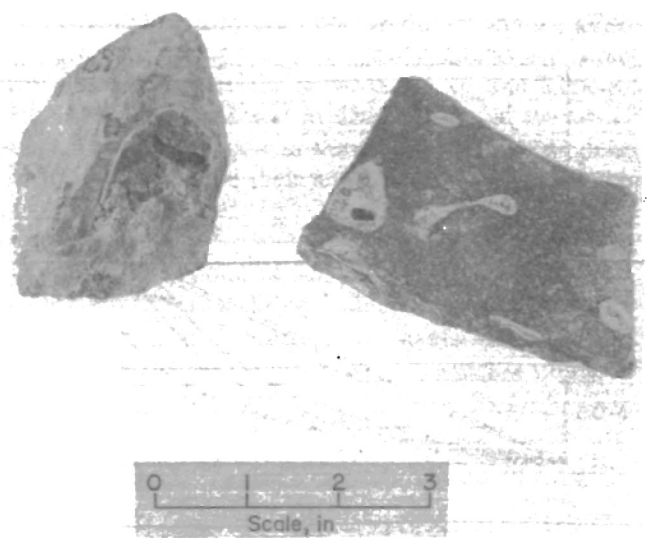

Figure 16.—Example of contact points identified by white splotches on rock.

$$E_s = \frac{\sigma}{\epsilon}, \quad (15)$$

$$E_t = \frac{\Delta\sigma}{\Delta\epsilon}, \quad (16)$$

where E_s = secant modulus, psi,

E_t = tangent modulus, psi,

σ = cumulative vertical stress, psi,

ϵ = cumulative strain, in/in,

$\Delta\sigma$ = change in vertical stress, psi,

and $\Delta\epsilon$ = change in strain, in/in.

A spreadsheet software program was used to calculate the secant and tangent moduli values at each point. These moduli values were graphed versus vertical stress and void ratio, curves were fitted to portions of the curves, and best fit equations were determined (based on stress level) as tabulated in table 5.

The tangent modulus versus stress is utilized to define the parameters used in the numerical model's stress-strain equation. According to another theory, the secant modulus versus stress is used to define the parameters of the stress-versus-strain curve. Consequently, both types of moduli were determined, and the two different theories are discussed in the section "Comparison of Theoretical Solutions With Test Results."

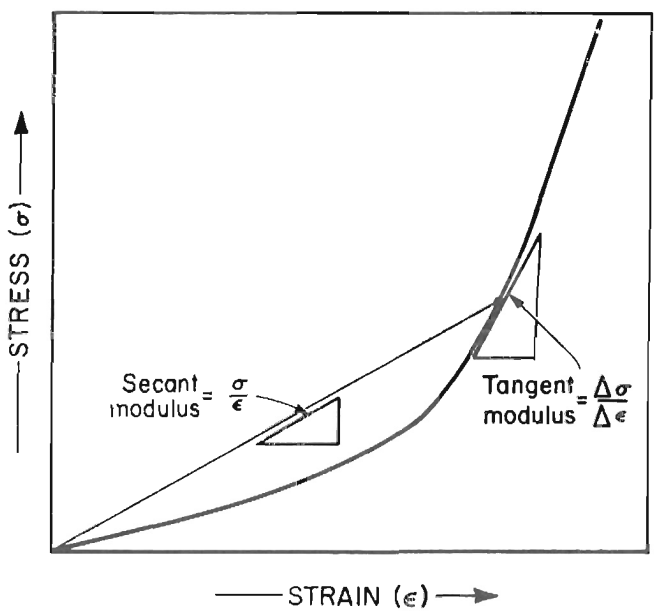

Figure 17.—Examples of secant and tangent moduli determination.

Table 5.—Equations of best fit curves for secant and tangent moduli versus stress

Test	Secant modulus versus stress		Tangent modulus versus stress			
	Best fit equation, linear fit [1]	r^2	Best fit equation, linear fit[2]	r^2	Best fit equation, second-degree polynomial fit[3]	r^2
			SHALE			
7	$2.29\sigma + 698$	0.99	$10.3\sigma + 975$	0.98	$0.00445\sigma^2 + 6.7\sigma + 562$	0.99
8	$2.27\sigma + 613$	.99	$9.9\sigma + 1{,}219$	.99	$.00387\sigma^2 + 7.31\sigma + 214$	.99
9	$2.25\sigma + 1{,}480$	.99	$11.1\sigma + 438$	.98	$.000783\sigma^2 + 9.83\sigma - 124$	.99
10	$2.36\sigma + 1{,}350$	.99	$11.7\sigma + 1{,}160$	.99	$.000306\sigma^2 + 11.6\sigma - 280$	.99
16	$2.09\sigma + 1{,}470$	.99	$11.6\sigma + 795$	.99	$.000197\sigma^2 + 11.1\sigma - 119$	.99
17	$2.29\sigma + 1{,}060$	.99	$11.9\sigma + 945$	.99	$.000690\sigma^2 + 10.9\sigma - 13.3$	.99
Av	$2.26\sigma + 1{,}110$	.99	$11.1\sigma + 922$	.99	$.00172\sigma^2 + 9.60\sigma + 40.0$	.99
			WEAK SANDSTONE			
11	$2.56\sigma + 1{,}470$	0.99	$14.7\sigma + 1{,}017$	0.99	$0.00215\sigma^2 + 10.3\sigma - 90.9$	0.99
12	$2.46\sigma + 1{,}260$	.99	$14.7\sigma + 1{,}006$	.99	$.00162\sigma^2 + 11.7\sigma - 657$	.99
13	$2.53\sigma + 1{,}290$	.99	$15.2\sigma + 850$	.98	$.00207\sigma^2 + 10.8\sigma - 91.9$	.99
14	$2.39\sigma + 1{,}080$	.99	$15.2\sigma + 344$	.99	$.00256\sigma^2 + 10.2\sigma - 259$	.99
15	$2.53\sigma + 1{,}600$	.99	$14.3\sigma + 611$	.97	$.00217\sigma^2 + 9.59\sigma + 136$	.98
Av	$2.49\sigma + 1{,}340$	.99	$14.8\sigma + 765$	.98	$.00211\sigma^2 + 10.5\sigma - 192$	.99
			STRONG SANDSTONE			
18	$2.41\sigma + 1{,}590$	0.99	$11.0\sigma + 1{,}620$	0.97	$0.000978\sigma^2 + 9.1\sigma + 902$	0.98
19	$2.36\sigma + 1{,}850$	.99	$10.9\sigma + 649$	.98	$.00171\sigma^2 + 6.26\sigma + 1{,}816$	.99
20	$2.27\sigma + 2{,}240$	.99	$10.5\sigma + 456$	.96	$.00185\sigma^2 + 5.27\sigma + 2{,}120$	.98
Av	$2.34\sigma + 1{,}890$	.99	$10.8\sigma + 908$	.97	$.00152\sigma^2 + 6.87\sigma + 1{,}612$	.98
Total av	$2.36\sigma + 1{,}360$	.99	$12.3\sigma + 865$	.98	$.00181\sigma^2 + 9.33\sigma + 294$	.99

r^2 Coefficient of determination.
[1]Used for average stress-secant modulus curve and for Salamon's equation.
[2]Used for Terzaghi's equation.
[3]Used for average stress-tangent modulus curve.

ANALYSIS OF RESULTS

Laboratory test results presented in figure 18 show that the averaged stress-strain behavior of the simulated gob material is nonlinear, which compares well with results of other compression tests of granular material (*6*). Figure 19 shows the variability between the actual test data and the best fit curve. Test results for the strong and weak sandstone have minimal variability, while the results for shale are slightly more scattered. It is interesting that at the lower stress levels the stress-versus-strain curve is approximately linear, which would explain the linear stress-strain behavior obtained by Wardle (*7*).

During the initial portion of the test, the rate of change of the stress-strain curves (tangent modulus) is greatest for the strong sandstone, followed by the weak sandstone and the shale. However, as strain hardening occurs, the tangent modulus increases more rapidly for the weak sandstone, followed by the shale and then the strong sandstone. Examination of the curves for secant modulus versus stress show that all stress levels are greatest for strong sandstone, followed by the weak sandstone and the shale. These phenomena are depicted in figure 18 at low and high stress levels. To better illustrate the stress-strain behavior of the rock, the individual moduli values were plotted versus the corresponding stress level and the void ratio.

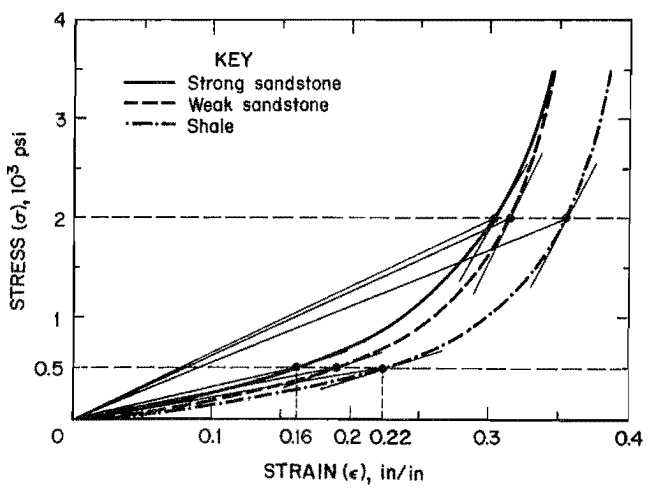

Figure 18.—Stress-versus-strain results—best fit curves. At 500 psi, pivotal stress level corresponds to strain range of 0.16 to 0.22.

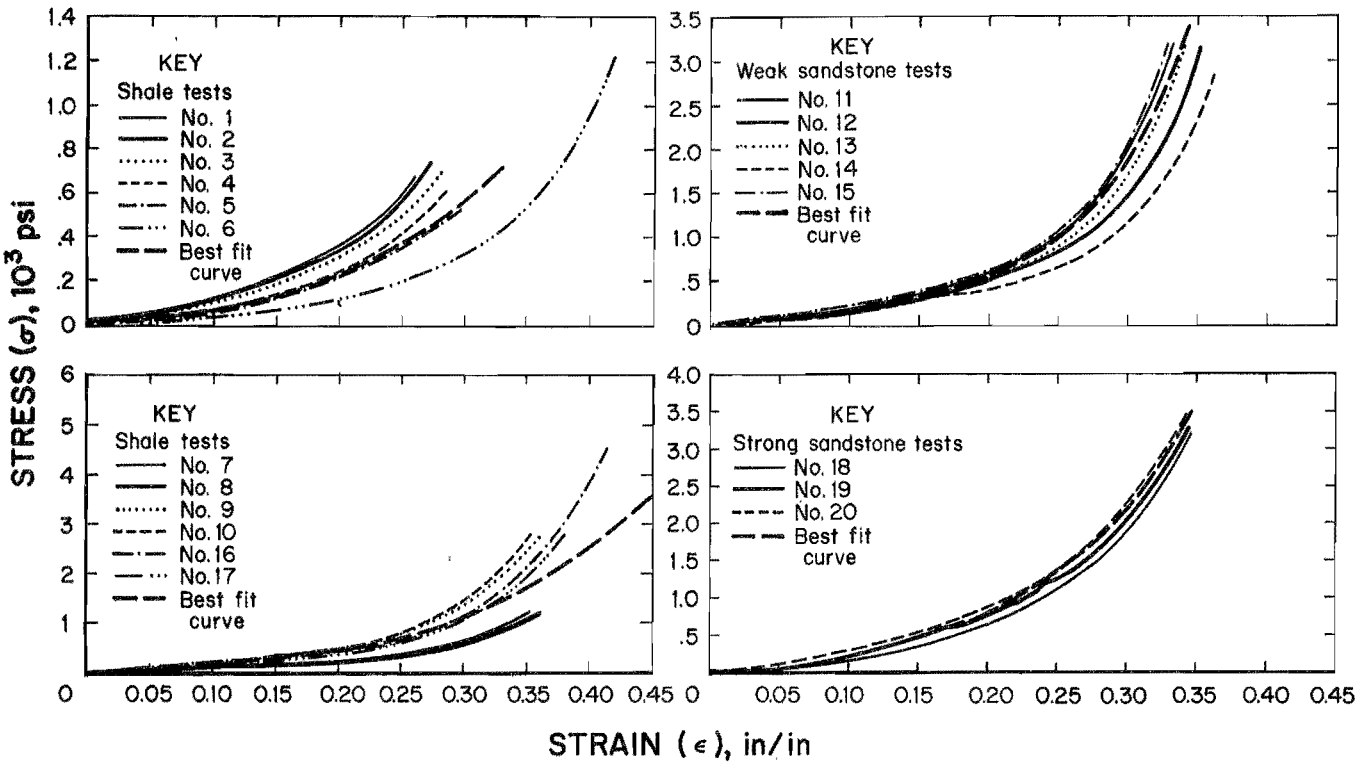

Figure 19.—Stress-versus-strain results—actual data for each test.

STRESS LEVEL

Plotting of the secant-modulus-versus-stress level (fig. 20) produces a perfectly linear curve, while plotting the tangent-modulus-versus-stress level (fig. 21) results in a nonlinear, second-order polynomial curve. These curves replicate the behavioral patterns presented in the previous paragraph. The secant modulus curves show that the rock types are clustered; the highest curve is the strong sandstone, followed by the weak sandstone and the shale. The rock type curves for the tangent modulus are somewhat clustered, especially between the 0- and 2,000-psi stress levels. As the insert in figure 21 shows, the strong sandstone initially produces the highest tangent modulus values, followed by the shale and weak sandstone, possibly indicating that the strong sandstone has a stiffer initial skeletal structure. However, the rock types reverse this order at a pivotal point of 500 psi.

It is interesting that the equivalent amount of strain that occurs at the pivotal point on the stress-strain curve in figure 18 ranges from 0.16 to 0.22 in/in, which is similar to the 22-pct initial compaction estimated by Su (*16*).

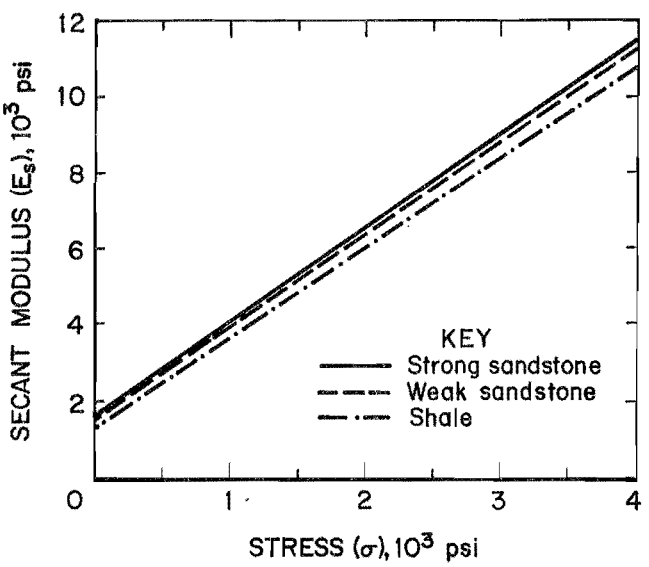

Figure 20.—Stress versus secant modulus averaged for each rock type.

The equations for these moduli-versus-stress curves are listed for each individual test in table 5. Inserting an estimated stress level of 800 psi into these equations produces moduli values as shown in table 6. These values seem to compare favorably with the in situ test results and are somewhat lower than the other laboratory test results shown in table 1.

Table 6.—Moduli results at 800-psi stress level[1]

Rock type	Modulus, psi	
	Secant	Tangent
Shale	2,920	8,820
Weak sandstone	3,330	9,560
Strong sandstone . . .	3,760	8,080

[1]Based on average equations in table 5.

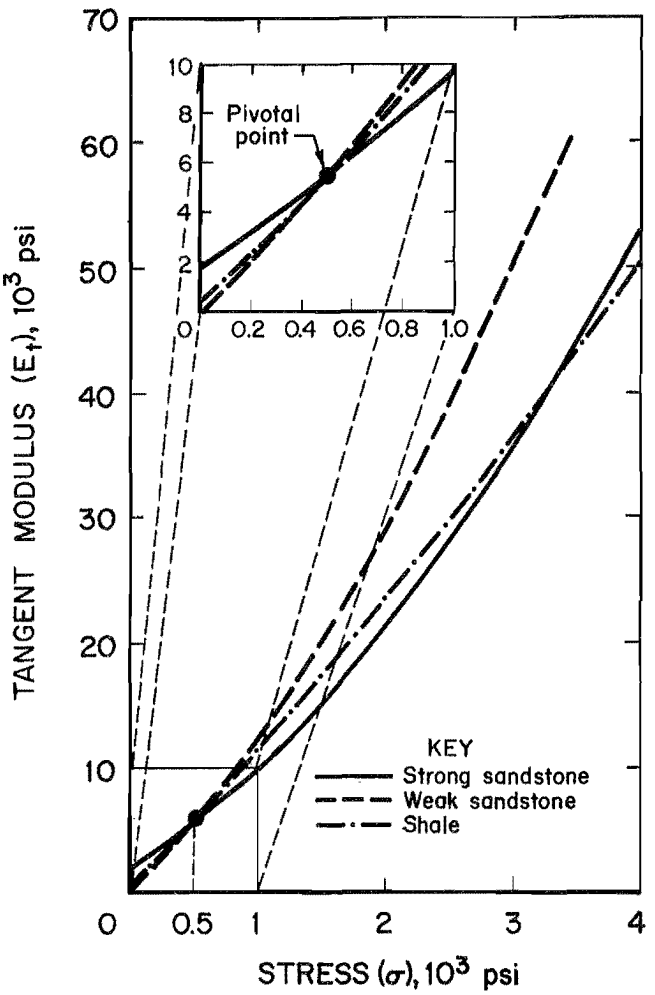

Figure 21.—Stress versus tangent modulus for each rock type. Insert shows pivotal point at 500 psi where all rock types converge.

In comparing the test results in table 6, the type of rock tested does not appear to dramatically affect the resulting moduli values, considering the wide range of rock types used in the tests. Consequently, a first approximation of the secant and tangent moduli can be based on the averaged results for all three rock types. Figure 22 shows the averaged linear curve of the secant modulus and the averaged second-order polynomial curve of the tangent modulus based on the stress level, as well as the equations and ranges of these averaged moduli curves. Also evaluated was the correlation of determination (r^2), which measures the proportion of the variation in the best fit equation that is explained through knowledge of the actual data. An $r^2 = 0.95$ was determined for the best fit curve for the secant modulus versus stress, and the best fit curve for the tangent modulus versus stress resulted in an $r^2 = 0.99$.

VOID RATIO

Plotting the secant and tangent moduli versus the void ratio resulted in the third-order polynomial best fit curves shown in figure 23. All three rock types produced distinctly separate curves. Both moduli plots generated consistent curves, with $r^2 = 0.905$ to 0.984 for the secant modulus curves and $r^2 = 0.969$ to 0.979 for the tangent modulus curves. The strong sandstone curve consistently produced the highest modulus values, followed by the weak sandstone and the shale.

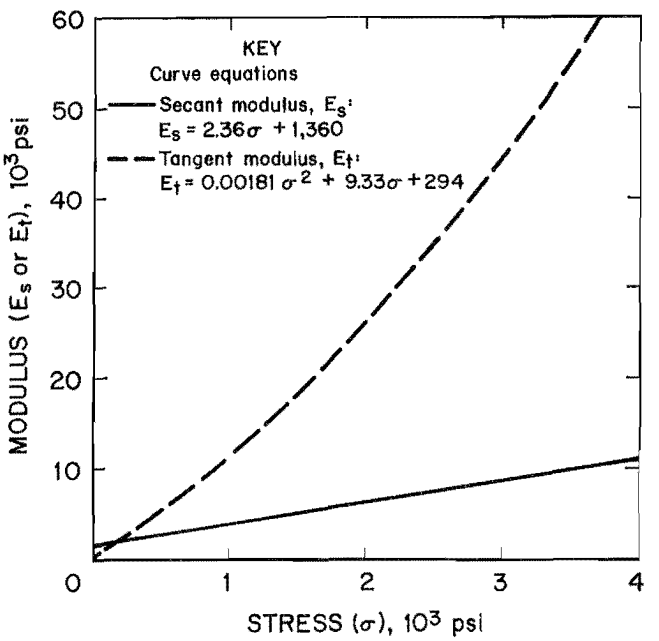

Figure 22.—Stress versus secant and tangent moduli curves and equations averaged from all rock types.

Initial trends of the tangent modulus curve (fig. 23) show that the modulus stays constant until it reaches avoid ratio of 0.40 for the shale and weak sandstone and about 0.55 for the strong sandstone. The equivalent strains at these void ratios range from 0.16 to 0.22, which are similar to the strains identified on figure 18 using the pivotal point of 500 psi identified on figure 21. At this initial stage of the test, the rock modulus is not changing during the compaction process. This may indicate that the simulated gob material is maintaining its skeletal stiffness even though the void ratio is changing because of slippage of the rock pieces. This same behavior pattern was not as distinctly identified for the secant modulus curves (fig. 23).

In the later stage of the test, the secant and the tangent moduli curves for all of the rock types increase exponentially with decreasing void ratio (fig. 23). It is probably at this stage that strain hardening occurs, when the higher confinement and normal stresses produce less slippage (because of higher friction) and more rock breakage, filling a majority of the voids. The filling and compaction of the void space increases the stiffness of the rock matrix, thereby dramatically increasing the modulus of the material.

The relationship of the moduli to the void ratio appears to be associated with rock types, whereas the relationship of the moduli to the stress level was not as profoundly related to distinct rock types. Consequently, it was determined to investigate how statistically significant the rock type and other parameters, such as the particle size, are in affecting the outcome of the test. Two statistical methods utilized were analysis of variance (ANOVA) and multiple regression analysis.[7]

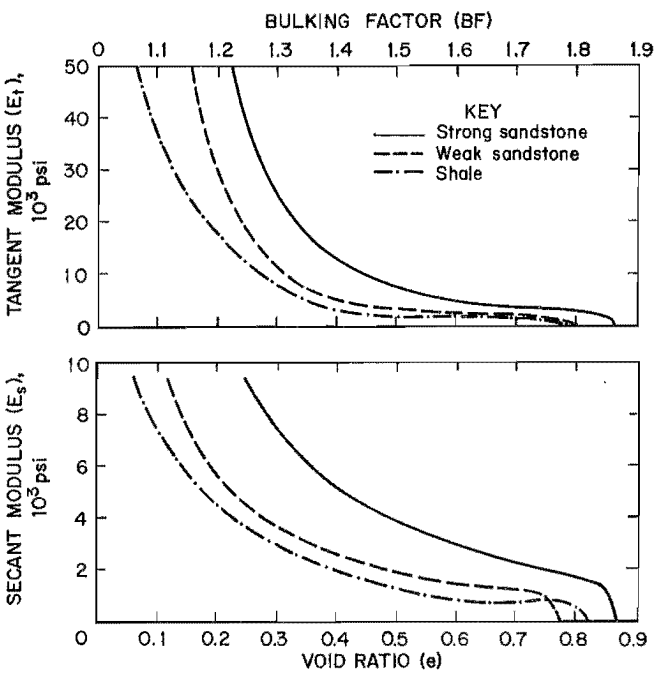

Figure 23.—Void ratio versus secant and tangent moduli for all rock types.

ANALYSIS OF VARIANCE

ANOVA is used to determine whether a set of test results are statistically different. The ANOVA test, if a significant difference exists between the sample means (using the F-ratio), gives an indication if the samples were drawn from the same population. The null hypothesis for this test states that the samples have been drawn from the same population, and the test is applied to see if the null hypothesis can be rejected at a given significance level (*32*). The significance level selected for all tests was 0.05 (i.e., probability $\leq$ 0.05), which is equivalent to a 95-pct confidence level.

The ANOVA was applied to the test results to determine if the rock type or maximum particle size significantly affects the variables, such as void ratio, particle breakage, final shape ratio, secant modulus, and tangent modulus. The null hypothesis for these tests was that changing the rock type or particle size does not significantly change the variables. Table 7 shows the significance levels at which the null hypothesis can be rejected, and the asterisks indicate variables with respective significance levels less than 0.05 (95-pct confidence interval). The results suggest that the void ratio, secant modulus, tangent modulus, and most of the shape ratios are significantly affected by changing the rock type. On the other hand, changes in the maximum particle size do not significantly affect any of the variables. Table 8 displays the averaged values and standard deviations of the factors that were determined significant from the ANOVA for results at equivalent load levels.

Particle Size

As suggested by the ANOVA results in table 7, none of the factors were significantly affected by the change in maximum size of the simulated gob material. To verify this statistical evaluation, the average percent compaction at a stress level of 500 psi was evaluated for tests using various maximum particle sizes. Table 9 shows that the percent compaction is unaffected by varying the maximum particle size. However, compaction did seem to be affected by the shape of the gob gradation curve. Compaction results for test 6, presented in table 4, appear to be significantly different from results of other tests. This difference is attributed to the dissimilar gradation curve

[7]The authors are grateful to Richard Jones, geologist, Pittsburgh Research Center, for his assistance with the statistical software program that evaluated the ANOVA and multiple regression analysis.

that was used for test 6, suggesting that the shape of the grain size distribution curve may affect the compressibility of the simulated gob material (see appendix figure A-1, the shape of the gradation curve for test 6 versus the curves for the other tests). This implies that the test results are most applicable when the gradation of the actual gob is similar to the laboratory gradation curve shown in figure 8.

Table 7.—ANOVA test results,[1] showing variables or parameters significantly affected

Variable or parameter	Significance level	
	Rock type[2]	Maximum particle size[3]
Void ratio:		
Initial	0.0258*	0.4609
At 800 psi	.0000*	.2201
Final	.0413*	.8219
Percent compaction	.0199*	.9863
Particle breakage	.2345	.4084
Shape ratio before:		
Thickness to width	.0167*	NAp
Width to length	.0243*	NAp
Shape ratio after:		
Thickness to width	.0000*	NAp
Width to length	.3263	NAp
Tangent modulus:[4]		
Stress level	.0040*	.2953
Bulking factor	.0500*	.0806
Secant modulus:[4]		
Stress level	.0079*	.2471
Bulking factor	.0157*	.1802

NAp Not applicable.

[1]Includes data from all tests except test 6.

[2]Asterisk denotes significance level ≤0.05 (confidence level of 95 pct that the factor significantly affects results).

[3]Based on data derived from best fit curve at a stress level of 800 psi or, indirectly, the equivalent bulking factor at 800 psi.

NOTE.—ANOVA was also conducted on the shape ratio before the test versus the shape ratio after the test. Results showed that the thickness-to-width ratio had a significance level of 0.0167* and the width-to-length ratio had a significance level of 0.2630.

Rock Type

Unlike particle size, the rock type was significantly correlated with a number of output parameters. The compressibility (percent compaction and void ratio), modulus, and particle shape were found to be a function of the type of rock used in the test (table 7). It should be noted that "rock type" is a more generic term for other parameters uniquely associated with the rock, such as its composition, compressive strength, and surface texture.

Compressibility

As the ANOVA results show, the rock type significantly affects all of the parameters associated with the compressibility of the rock. The percent compaction or strain of the rock at equivalent maximum loads shows that most of the deformation occurs during the early stage of the test (fig. 18). The strong sandstone had the highest initial void ratio, followed by the shale and weak sandstone (table 8). At a stress level of 800 psi, the void ratio of the weak sandstone had surpassed that of the shale. The final void ratio repeated this same trend, indicating that the shale was the most compressible material, followed by the weak sandstone and strong sandstone. This trend was confirmed with the percent compaction, which determined that the shale had the highest percent compaction with 36 pct, followed by the weak and strong sandstone (34 and 33 pct, respectively). Although the particle breakage was found not to be a significant factor with the ANOVA analysis, it displays a similar trend, with shale producing the highest particle breakage followed by the weak sandstone and strong sandstone (table 8).

The rock compressibility may also be affected by the rock strength. The strong sandstone had an overall compressive strength of 16,400 psi, while shale and weak sandstone had considerably lower strengths of 8,000 and 6,300 psi, respectively. Therefore, stronger rock can be associated with less compaction, less particle breakage, and higher final void ratios. Particle shape may also affect the degree of compaction; this is discussed in the next section.

Some of the tests evaluated the amount of strain reduction when the test material was being unloaded (however, the numbers were too few for statistical analysis), and it is interesting that under the same maximum loading the strong sandstone rebounded an average of 1.58 pct while the shale rebounded only 0.85 pct (table 8). Possibly this shows that the strong sandstone is more capable of storing strain energy than are the other rock types.

Particle Shape

The ANOVA analysis in table 7 found that all of the shape ratios were significantly affected by rock type, with the exception of the after-test width-to-length shape ratio. Using Zingg's method (*25-26*) for classifying rock shapes, each rock type, prior to testing, had a slightly different shape (fig. 15): The shale is a disk shape, the weak sandstone borders on disk-spherical shape, and the strong sandstone borders on disk-blade shape. These shape differences are probably due to the unique crystalline structure of each rock type, which influences the fracturing of the rock. As figure 24 depicts, the strong sandstone is rectangular with sharp, defined corners, the weak sandstone is slightly more spherical in shape with smooth, rounded corners, and the shale is flat with feathered edges and many irregular corners. The average initial void ratio of each rock type (table 8) shows that the weak sandstone is the most densely packed, probably because of its

spherical shape, which will pack more tightly together than will the rectangular-shaped strong sandstone and disk-shaped shale. However, the weak sandstone exceeded the shale's void ratio at 800 psi and the final void ratio, indicating that the thinner, irregularly shaped shale pieces were breaking more and producing more particle breakage than the weak sandstone (this point is evident by the higher particle breakage for shale shown in table 8).

Following completion of the load deformation tests, the shape ratios were evaluated and compared with the before-test shape ratios using the ANOVA. Results in the note under table 7 show that there is a significant difference in the thickness-to-width shape ratio, but not in the width-to-length ratio. Apparently, the width and length of the rock particles were breaking proportionally while the thickness (smallest dimension) of the broken rock pieces was becoming proportionally larger, indicating a more spherical-shaped rock following the test. Figure 15 shows that the strong sandstone changed the most in shape, starting with a blade-disk shape and ending with a disk-spherical shape, indicating that the sharply defined edges of the rectangular pieces were being rounded off. The high strength of the strong sandstone prevented further breakage, resulting in less compaction of the material, as shown in table 9. The shale and the weak sandstone changed less in shape, but moved toward the spherical portion of the chart.

Table 8.—Averaged test results

	Shale		Weak sandstone		Strong sandstone	
	Av	Std dev	Av	Std dev	Av	Std dev
Void ratio:						
Initital	0.7950	0.0714	0.7426	0.0394	0.8667	0.011
At 800 psi	0.2958	0.0443	0.3232	0.0155	0.4877	0.0145
Final	0.1522	0.0514	0.1536	0.00086	0.2524	0.0067
Percent compaction	36.42	0.9440	34.30	1.40	33.23	1.84
Particle breakage[1]	179.0	42.56	163.6	42.92	127.8	9.15
Percent rebound[2]	0.85	0.188	1.17	0.0614	1.58	0.158
Shape ratio before:						
Thickness-to-width	0.4355	0.0234	0.6302	0.0443	0.5420	0.0362
Width-to-length	0.7022	0.0463	0.7356	0.0439	0.6730	0.0111
Shape ratio after:						
Thickness-to-width	0.5295	0.0202	0.6688	0.0098	0.6740	0.0386
Width-to-length[1]	0.7183	0.0276	0.7336	0.0262	0.7053	0.0162
Tangent modulus,[3] psi:						
Stress level	8,780	554.8	8,133	254.9	7,178	770.3
Bulking factor	8,363	736.2	7,588	427.3	7,335	585.8
Secant modulus,[3] psi:						
Stress level	2,918	367.5	3,334	247.2	3,768	443.8
Bulking factor	3,011	385.6	3,154	246.5	3,808	380.0

[1]Not determined significant with ANOVA analysis.
[2]ANOVA was not performed because of small sample size.
[3]Based on modulus values derived from best fit curve at a stress level of 800 psi, or, indirectly, the equivalent bulking factor at 800 psi.

Table 9.—Evaluation of maximum size effect on percent compaction at 500 psi for shale

Maximum size	*Compaction, pct*	*Maximum size*	*Compaction, pct*
2 in:		3 in-(cont.):	
Test 4	0.2656	Test 16	0.2150
Test 9	.2410	Test 17	.2290
Av	.2533	Av	.2448
Std dev	.0174	Std dev	.025
3 in:		3.5 in:	
Test 1	.2310	Test 5	.2880
Test 2	.2350	Test 10	.2060
Test 3	.2490	Av	.247
Test 7	.2690	Std dev	.058
Test 8	.2860		

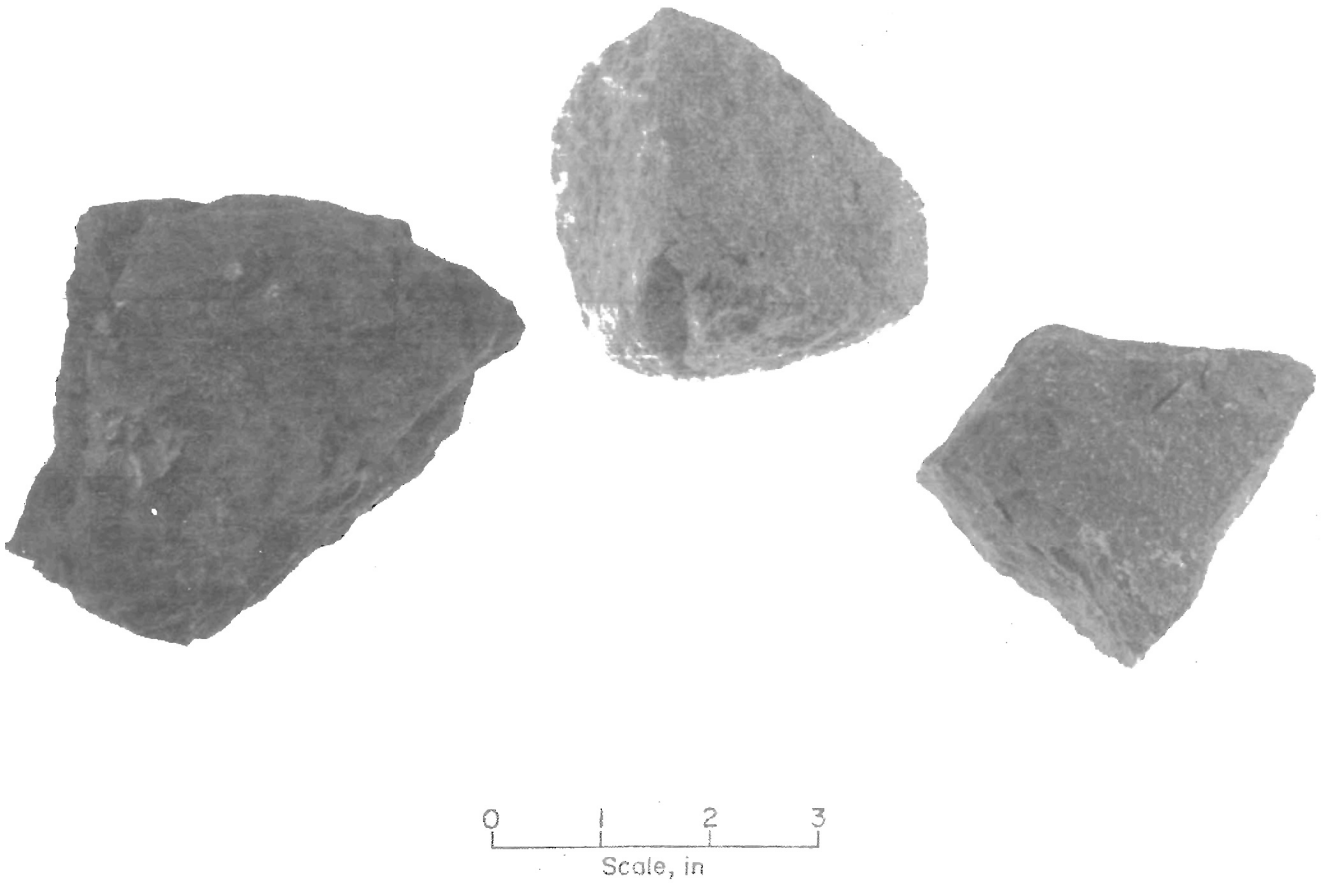

Figure 24.—Examples of three rock types and distinct shapes used in laboratory tests, left to right: shale (disk shape), weak sandstone (disk-spherical shale), and strong sandstone (disk-blade shape).

Also possibly related to the shape effect was the average number of contact points prior to testing. Weak sandstone had an average number of 5.20 contact points, followed by shale and strong sandstone with 4.74 and 4.68, respectively. The higher number of contact points for the weak sandstone may indicate that the more spherical shape and denser packing resulted in more contact points between the rock pieces. The shale and strong sandstone had a slightly lower number of contact points, which may relate to the disk and rectangular shapes of the rock pieces, resulting in a looser packing of the rock and a higher initial void ratio.

Modulus

The ANOVA results in table 7 show that rock type significantly affects the outcome of the secant and tangent moduli values based on both stress level and void ratio. Therefore, the initial assumption that the secant and tangent moduli could be estimated based on the stress level (fig. 22) independent of the rock type may be inexact. Since differences among rock type moduli are very small (table 6), in comparison to the large range of values used in past modeling situations (table 2), these minimal differences will have a negligible effect on the numerical model results. For an approximation of a rock modulus similar to the rock type and gradation used in these tests, figure 22 is adequate; however, for estimating the modulus of a rock type different from the laboratory rock, this figure may not be appropriate. Since the rock types used in this laboratory study will not match identically the rock types found in most gobs, a means of characterizing the rock types needs to be established.

MULTIPLE REGRESSION ANALYSIS

To evaluate the input parameters that characterize the rock type and to produce a predictive method of estimating the modulus, multiple regression analysis was found to be a useful tool. Multiple regression analysis is able to evaluate the relationship between one dependent variable and several independent variables. According to

Doornkamp (*32*), the purpose of multiple regression is to discover if variations in values of a particular variable are accounted for more by its relationship to two or more other variables taken together than to any one individual variable. The advantage of multiple regression is that after it selects the independent variables that best predict the dependent variable, it produces an equation for predicting the dependent variable given the independent variables.

Secant and Tangent Moduli

Using a statistical software package, multiple regression analysis evaluated several independent parameters (i.e., rock strength, shape ratios, particle breakage, and initial void ratio) with respect to the tangent modulus at a wide range of bulking factor values. This analysis was duplicated using the secant modulus values. Results of the analysis show that both the secant and tangent moduli are a function of the rock strength and thickness-to-width shape ratio with a fairly high degree of correlation (i.e., the multiple coefficient of determination or R^2 = 0.84 to 0.94). Equations were formulated to predict the tangent modulus and secant modulus at various bulking factors given the rock strength and thickness-to-width shape ratio, as shown in table 10. Because of constraints within the test data, the equations for the very high and very low bulking factors were extrapolated (BF = 1.15, 1.20, 1.60). Figures 25 and 26 show the plots of these equations at several different thickness-to-width shape ratios.

Trends in figures 25 and 26 for both the secant and tangent moduli analysis show that as the rock strength increases so does the modulus, and as the bulking factor decreases the modulus values increase. Also, as the shape ratio increases the modulus increases. The thicker and narrower rock has a higher modulus factor, perhaps because its competent shape results in a stiffer rock matrix.

Bulking Factor

Since the modulus was found to be a function of the rock strength and thickness-to-width shape ratio based on the bulking factor, a link was needed to connect the bulking factor to a more obtainable mine parameter such as the overburden stress level. Toward that end, another series of multiple regression analyses was conducted to determine the bulking factor based on the overburden stress level. The regression analyses evaluated the same independent variables (i.e., rock strength, shape ratios, particle breakage, and initial void ratio) with respect to bulking factors at various stress levels. Results of the analysis disclosed that the bulking factor is a function of the rock strength and thickness-to-width shape ratio, the same two variables found to be a function of the modulus. Again, the multiple coefficient of determination of the analysis was high (i.e., R^2 = 0.83 to 0.91). Equations were formulated to predict the bulking factor at various stress levels given the rock strength and thickness-to-width shape ratio, as shown in table 10. Figure 27 shows the plot of these equations graphed with rock strength versus the bulking factor at various stress intervals, with three plots, each representing different thickness-to-width shape ratios.

Table 10.—Multiple regression equations for predicting specified parameters

Level	Multiple regression equations	R^2
BULKING FACTOR (BF) AT VARIOUS STRESS LEVELS (σ)		
σ = 400 psi	BF = 0.0000184X1 + 0.267X2 + 1.16	0.828
σ = 600 psi	BF = 0.0000203X1 + 0.274X2 + 1.06	.875
σ = 800 psi	BF = 0.0000187X1 + 0.262X2 + 1.04	.873
σ = 1,000 psi	BF = 0.0000185X1 + 0.269X2 + 0.992	.892
σ = 1,500 psi	BF = 0.0000160X1 + 0.209X2 + 1.00	.901
σ = 2,000 psi	BF = 0.0000150X1 + 0.221X2 + 0.963	.908
σ = 2,500 psi	BF = 0.0000136X1 + 0.247X2 + 0.931	.894
TANGENT (E_t) MODULUS AT VARIOUS BULKING FACTORS (BF)		
BF = 1.25	E_t = 2.49X1 + 41,200X2 - 24,800	0.930
BF = 1.30	E_t = 1.76X1 + 23,800X2 - 15,700	.921
BF = 1.35	E_t = 1.32X1 + 16,300X2 - 11,400	.898
BF = 1.40	E_t = 0.933X1 + 11,300X2 - 7,900	.916
BF = 1.50	E_t = 0.568X1 + 6,900X2 - 5,000	.935
SECANT MODULUS (E_s) AT VARIOUS BULKING FACTORS (BF)		
BF = 1.25	E_s = 0.539X1 + 10,400X2 - 5,340	0.939
BF = 1.30	E_s = 0.445X1 + 7,760X2 - 4,160	.943
BF = 1.35	E_s = 0.348X1 + 5,580X2 - 2,750	.906
BF = 1.40	E_s = 0.283X1 + 4,900X2 - 2,300	.903
BF = 1.50	E_s = 0.348X1 + 5,580X2 - 2,750	.840

NOTE.—X1 is the rock strength parameter, X2 is the thickness-to-width shape ratio, and R^2 is the multiple coefficient of determination. The curves shown in figures 25 to 27 are based on these equations.

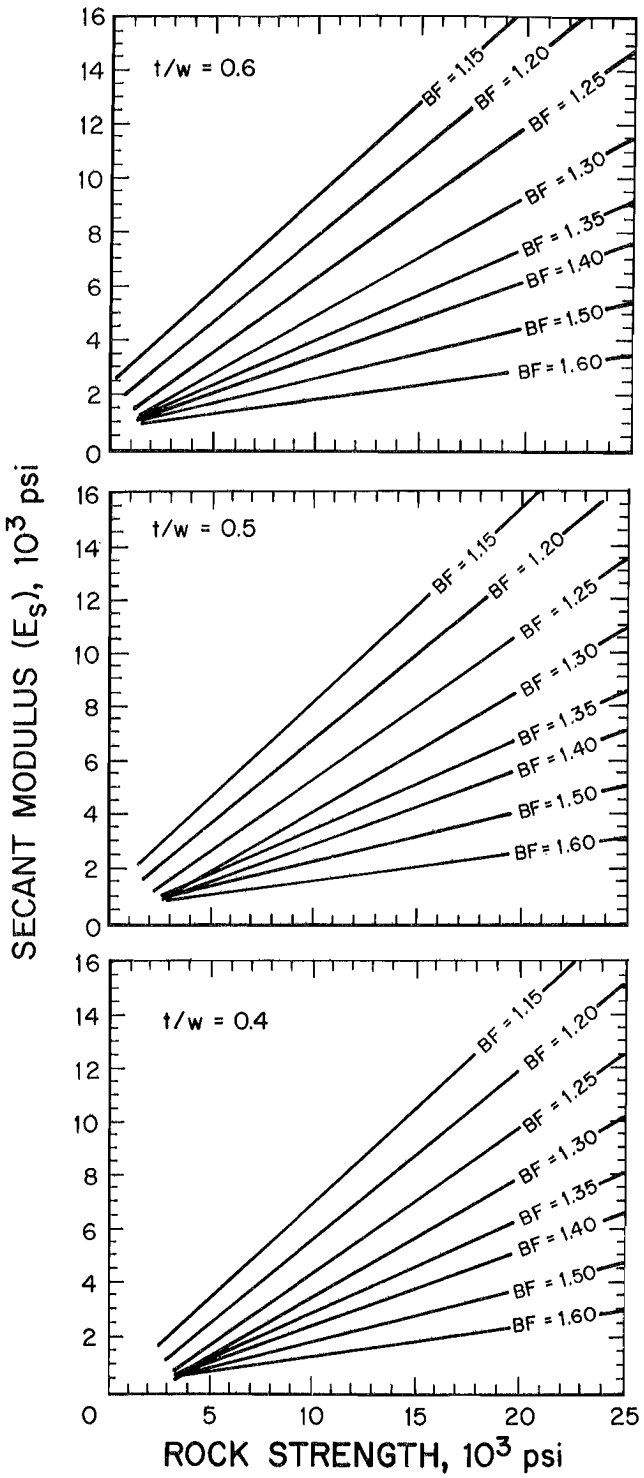

Figure 25.—Multiple regression curves—rock strength versus secant modulus for various thickness-to-width shape ratios.

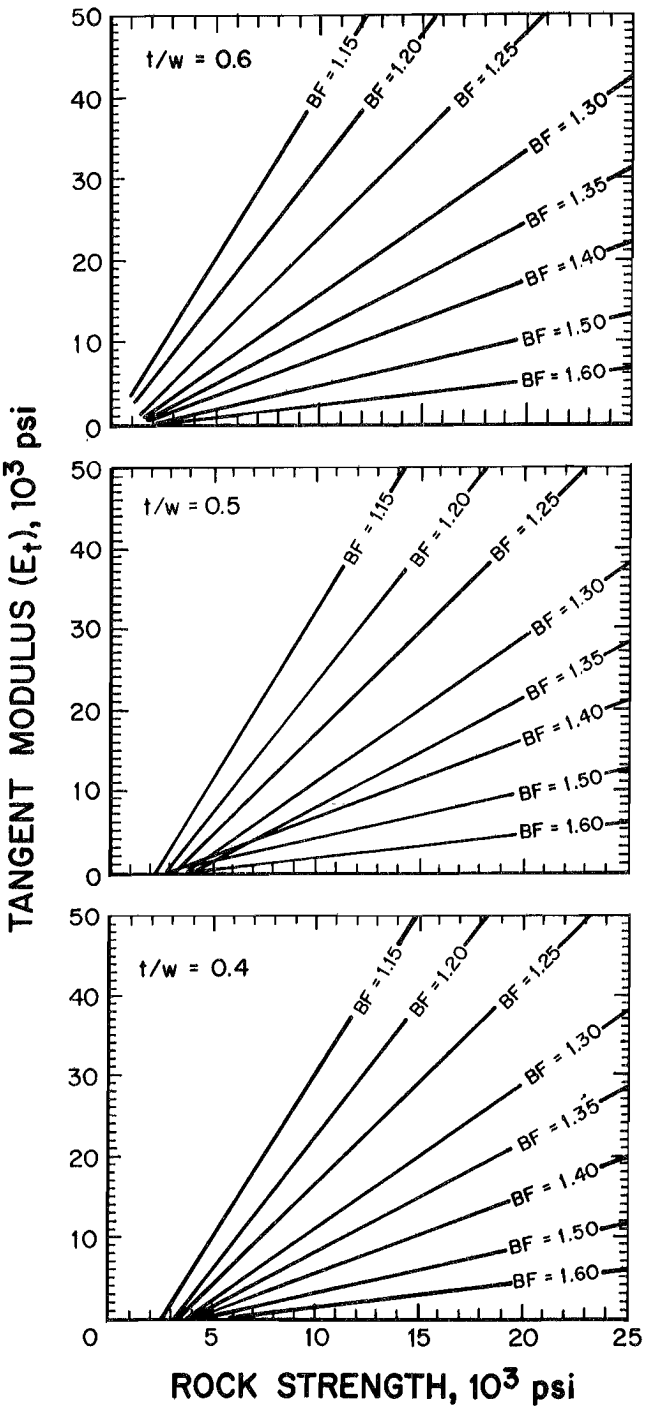

Figure 26.—Multiple regression curves—rock strength versus tangent modulus for various thickness-to-width shape ratios.

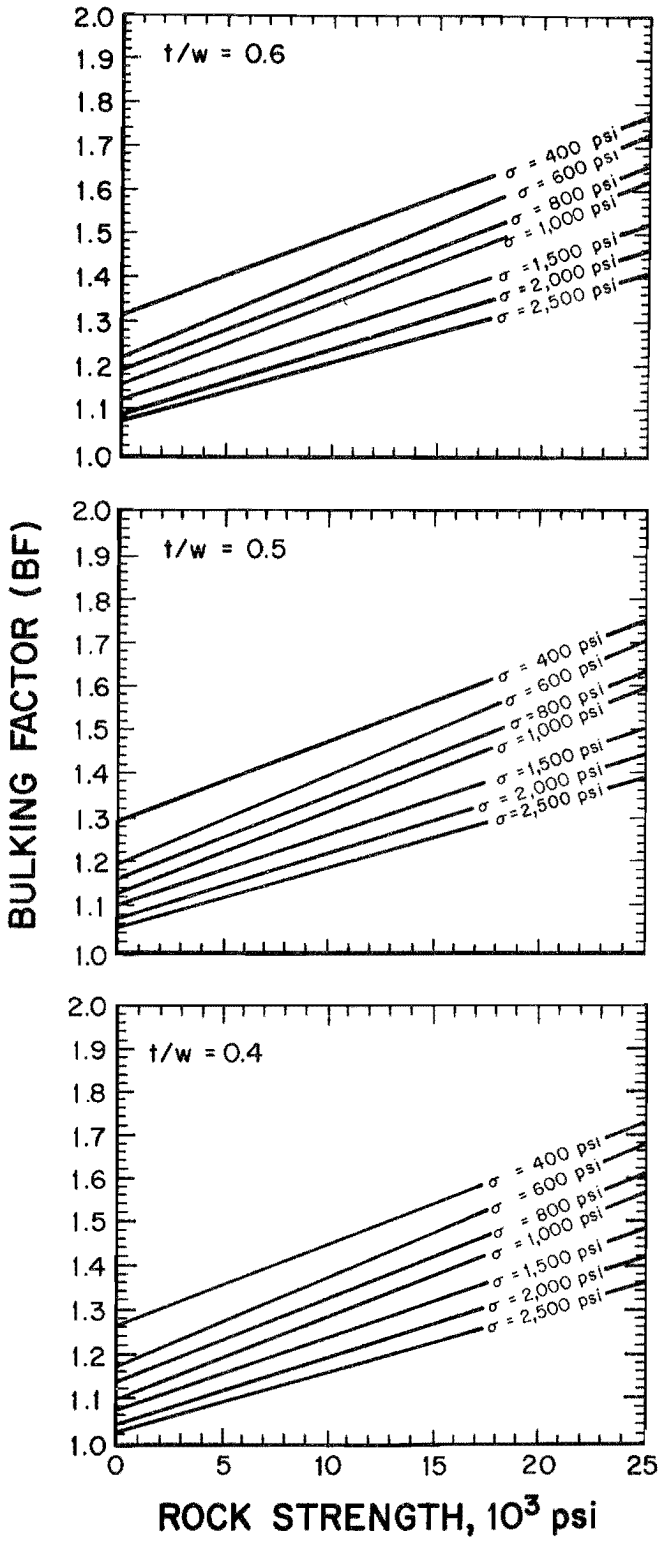

Figure 27.—Multiple regression curves—rock strength versus bulking factor for various thickness-to-width shape ratios.

These plots indicate that as the rock strength and thickness-to-width shape ratio increases the bulking factor increases. Also, as the stress levels increase the bulking factor decreases. These trends seem logical since the stronger rock remains more intact, resulting in a higher bulking factor. The thinner and wider disk-shaped rock has a lower bulking factor; perhaps its fragile shape results in more breakage and ultimately less void space.

COMPARISON OF THEORETICAL SOLUTIONS WITH TEST RESULTS

Two theoretical solutions that define the compressive behavior of granular material were compared with the actual test results. The stress-strain curves derived from these theoretical solutions are used in the numerical model to approximate the strain-hardening behavior of the gob. The following equations define the stress-strain behavior of granular materials based on different theories developed by Ryder (*33*), Salamon (*34*), and Terzaghi (as discussed by Salamon in reference 35).

Salamon's Solution

According to Salamon (*34*), the following stress-strain equation describes the compressive behavior of backfill material.

$$\sigma = \frac{E_0 \epsilon}{(1 - \epsilon/\epsilon_m)}. \qquad (17)$$

Solving this equation for strain:

$$\epsilon = \frac{\epsilon_m \sigma}{(\epsilon_m E_0 + \sigma)}, \qquad (18)$$

where σ = applied stress, psi,

E_0 = initial secant modulus, psi,

ϵ = strain, in/in,

and ϵ_m = maximum strain, in/in.

Differentiating the stress-strain relation (equation 17) produces the following tangent modulus equation ($E_t = d\sigma/d\epsilon$):

$$E_t = E_0 + \frac{2\sigma}{\epsilon_m} + \frac{\sigma^2}{\epsilon_m^2 E_0}, \qquad (19)$$

where E_t = tangent modulus, psi.

Using equation 18 and solving it in terms of the slope (σ/ϵ) defines the secant modulus of the stress-strain relation

$$E_s = \frac{\sigma}{\epsilon} = E_0 + \frac{\sigma}{\epsilon_m}, \quad (20)$$

where E_s = secant modulus, psi.

This linear equation defines the equation of a line and can be compared with the best fit equations of the laboratory-determined secant modulus results shown in table 5. Therefore, the constants established from the laboratory secant modulus fitted lines (table 5) can be associated with the constants in the theoretically determined solutions of equations 17 and 19, where the intercept defines the initial secant modulus (E_0) and the slope defines the reciprocal of the maximum strain ($1/\epsilon_m$).

Terzaghi's Solution

Terzaghi's approach (*35*) suggests that the tangent modulus of granular material is a linear function of the stress, as expressed by the following equation:

$$E_t = \frac{d\sigma}{d\epsilon} = E_0 + a\sigma \quad (21)$$

where E_t = tangent modulus, psi,

σ = stress, psi,

ϵ = strain, psi,

E_0 = initial tangent modulus,

and a = dimensionless constant.

Expressing equation 21 in terms of strain:

$$\frac{d\epsilon}{d\sigma} = \frac{1}{E_0 + a\sigma}, \quad (22)$$

and integrating produces the following stress-strain equation:

$$\epsilon = \frac{1}{a}\ln\left(1 + \frac{a}{E_0}\sigma\right). \quad (23)$$

Solving equation 23 in terms of stress yields:

$$\sigma = \frac{E_0}{a}\left(e^{\epsilon a} - 1\right). \quad (24)$$

Then, solving equation 24 in terms of the secant modulus (σ/ϵ):

$$E_s = \frac{\sigma}{\epsilon} = \frac{a\sigma}{\ln\left(1 + \frac{a}{E_0}\sigma\right)}. \quad (25)$$

Since Terzaghi's solution is based on the linear fit of the tangent modulus curve, the laboratory data for the stress-versus-tangent-modulus curves were fitted to linear curves. However, these linear fits resulted in negative intercepts, which required that the intercept be recalculated by slightly shifting the curve closer to the y-axis. Using the recalculated intercept, the data curves were refitted and a new slope was determined. The constants established from these best fit curves of the stress-versus-tangent-modulus curves are shown in table 5. As with Salamon's solutions, these constants can be associated with Terzaghi's equations (equations 24-25), where the intercept defines the initial tangent modulus (E_0) and the slope defines the constant (a).

Comparing Terzaghi's and Salamon's equations with the actual laboratory data shows that for the stress-versus-strain results Salamon's curve closely follows the actual curve while Terzaghi's curve is not aligned in two of the three rock types (figs. 28-30). The stress-versus-secant-modulus curves show a good linear fit that Salamon's equation constants were based upon; however, Terzaghi's nonlinear curve is slightly off (figs. 31-33). The stress-versus-tangent-modulus curves show a fairly close linear fit that Terzaghi's equation constants were based upon, and Salamon's equations are close to the actual laboratory results for stress levels less than 2,000 psi (figs. 34-36). Overall, it appears that both methods model the compressive behavior of granular material, with Salamon's method more closely fitting the laboratory data.

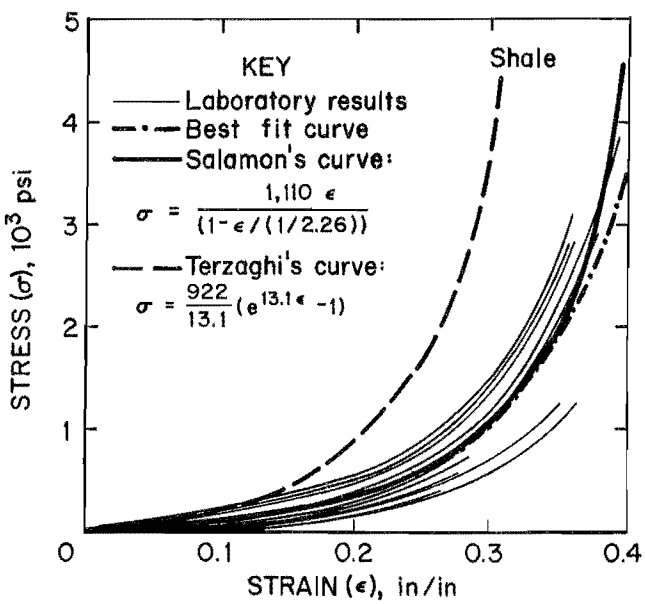

Figure 28.—Comparison of actual and best fit stress-versus-strain results with Salamon's and Terzaghi's theoretical solutions for shale.

Bureau of Mines
Report of Investigation 9458

BEHAVIOR OF SIMULATED LONGWALL GOB MATERIAL

By Deno M. Pappas and Christopher Mark

ERRATA

Replace figure 28 on page 26 with this corrected figure 28.

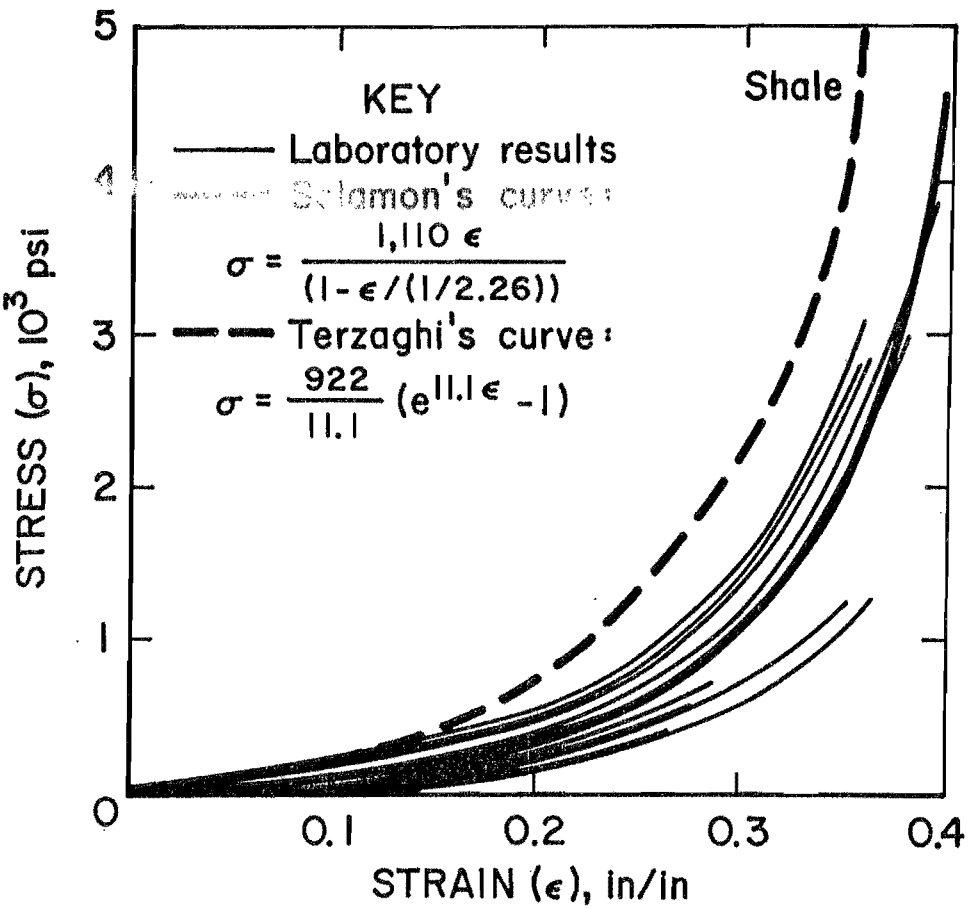

Figure 28.—Comparison of actual stress versus strain results with Salamon's and Terzaghi's theoretical solutions for shale.

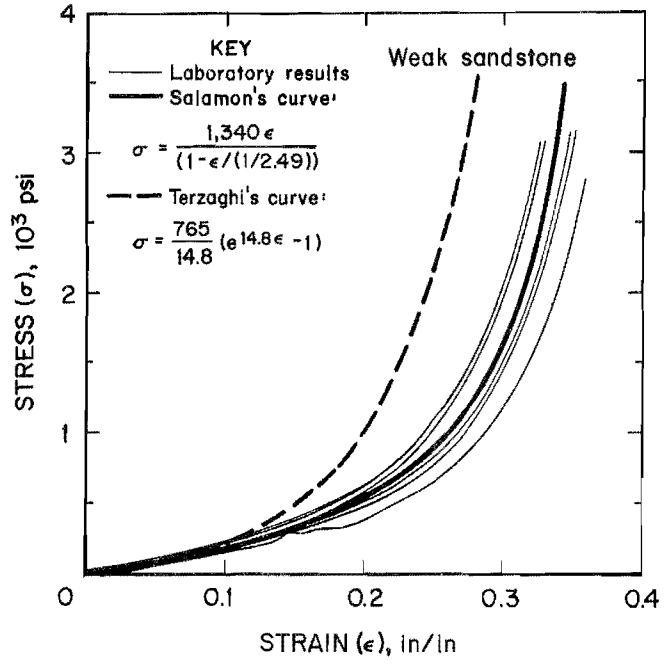

Figure 29.—Comparison of actual and best fit stress-versus-strain results with Salamon's and Terzaghi's theoretical solution for weak sandstone.

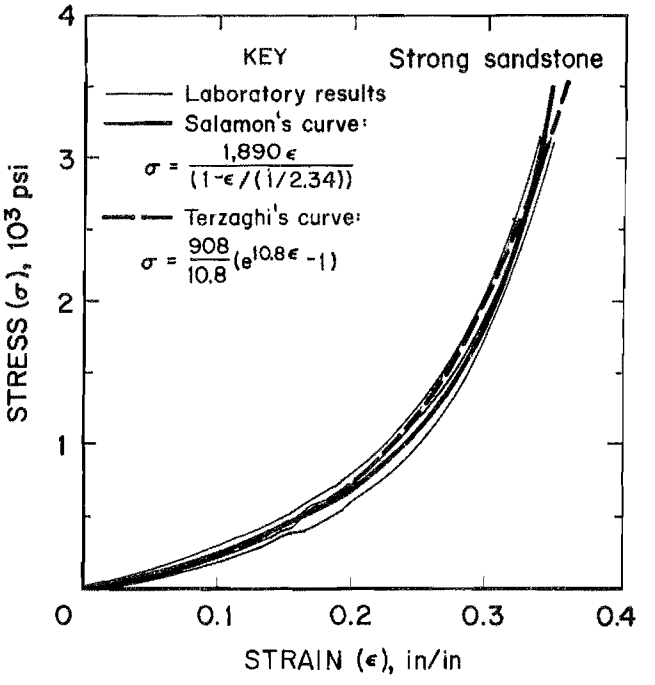

Figure 30.—Comparison of actual and best fit stress-versus-strain results with Salamon's and Terzaghi's theoretical solutions for strong sandstone.

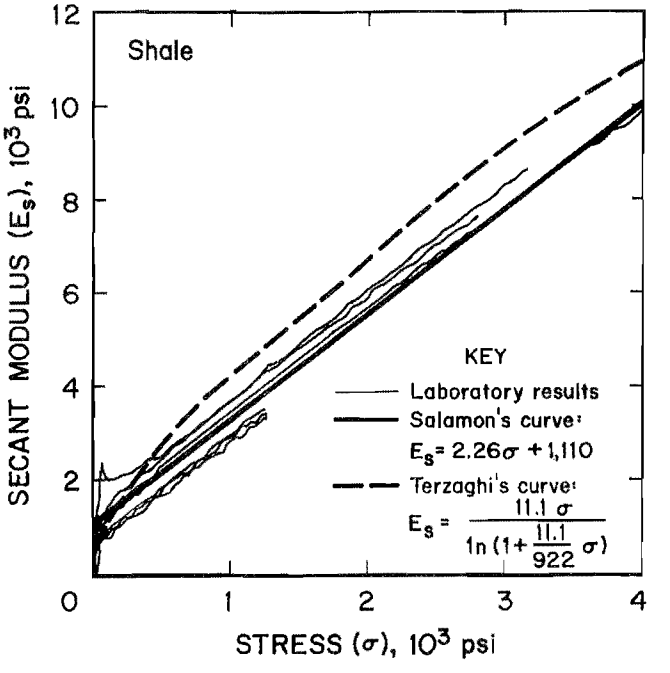

Figure 31.—Comparison of actual and best fit stress-versus-secant-modulus results with Salamon's and Terzaghi's theoretical solutions for shale.

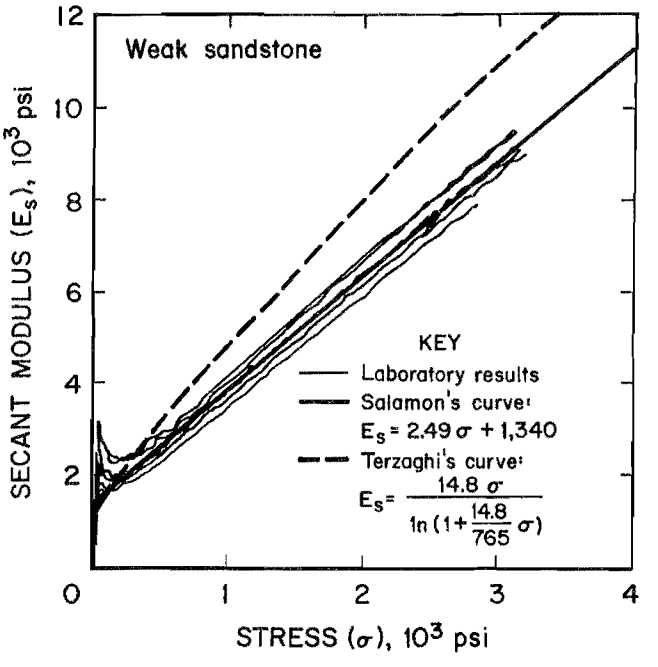

Figure 32.—Comparison of actual and best fit stress-versus-secant-modulus results with Salamon's and Terzaghi's theoretical solutions for weak sandstone.

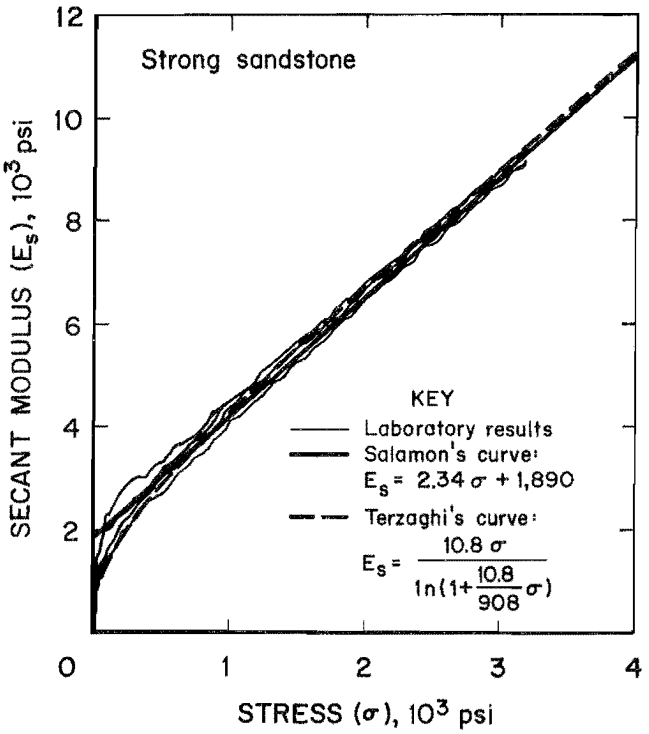

Figure 33.—Comparison of actual and best fit stress-versus-secant-modulus results with Salamon's and Terzaghi's theoretical solutions for strong sandstone.

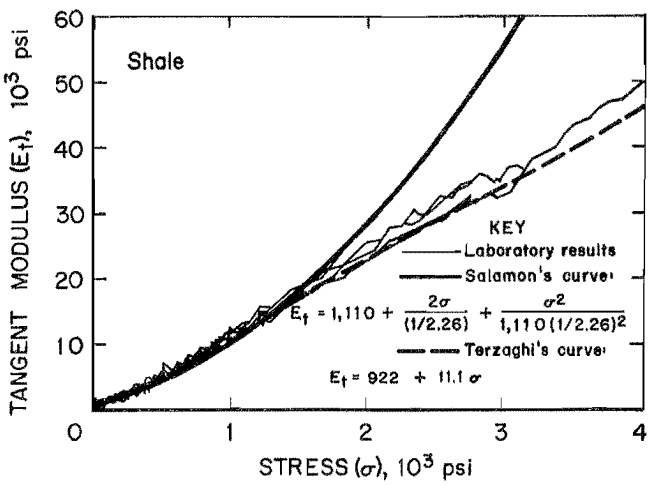

Figure 34.—Comparison of actual and best fit stress-versus-tangent-modulus results with Salamon's and Terzaghi's theoretical solutions for shale.

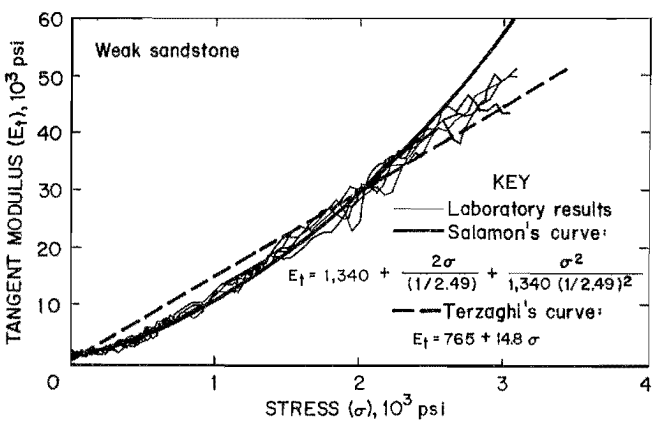

Figure 35.—Comparison of actual and best fit stress-versus-tangent-modulus results with Salamon's and Terzaghi's theoretical solutions for weak sandstone.

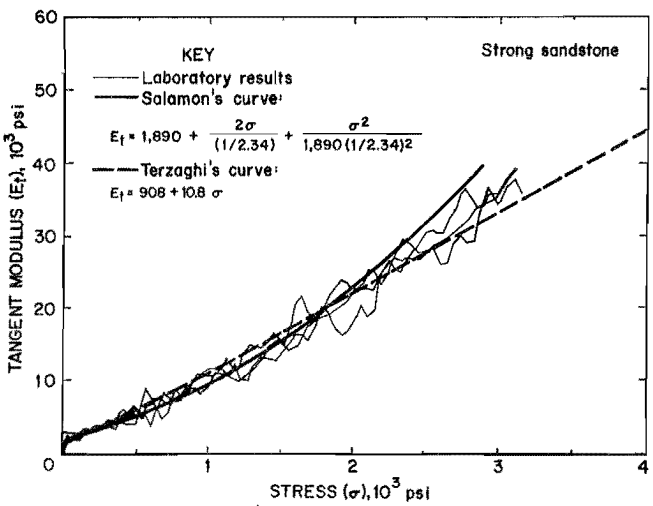

Figure 36.—Comparison of actual and best fit stress-versus-tangent-modulus results with Salamon's and Terzaghi's theoretical solutions for strong sandstone.

DISCUSSION

The intent of these laboratory tests was to provide a means for determining the modulus of the simulated gob materials for use in numerical modeling analysis. The first approximation used to determine the modulus was found to be a function of the stress level. The secant modulus versus stress level consists of the following equation:

$$E_s = 2.36\sigma + 1{,}360, \quad (26)$$

where E_s = secant modulus, psi,

and σ = stress level (due to overburden), psi.

The nonlinear behavior of the tangent modulus versus stress level is described in the following equation:

$$E_t = 0.00181\sigma^2 + 9.33\sigma + 294, \quad (27)$$

where E_t = tangent modulus, psi,

and σ = stress level (due to overburden), psi.

These equations and the curves are shown in figure 22.

For example, a mine with an overburden stress level of 680 psi produces a secant modulus of 2,970 psi and a tangent modulus of 7,410 psi according to the above equations.

A more exact estimate may be obtained from the multiple regression analysis of the test data. The multiple regression analysis produced several predictive curves that allow the bulking factor, tangent modulus, and secant modulus to be determined based on the rock strength, rock shape ratio, and stress level. If the stress level, the estimated shape ratio of the gob rock, and the compressive strength of the rock are known, the bulking factor can to be estimated using figure 27. With the estimated bulking factor known, the secant and tangent moduli can be determined from figures 25 and 26.

An example follows, using the data presented in the longwall caving height study conducted by Listak (*36*). The study was conducted in a mine with an overburden of 618 ft, or a stress level of 680 psi. The eventual gob was composed of the immediate roof, which was black shale with a compressive strength of 6,500 psi. Although the thickness-to-width shape ratio was unknown, for shale it was estimated to be about 0.45. Using figure 27 for a shape ratio of 0.4 and interpolating between the stress level curves at the rock strength of 6,500 psi yields a bulking factor of 1.295. Repeating this procedure for a shape ratio of 0.5 produces a bulking factor of 1.32. Averaging the bulking factors for the shape ratio of 0.45 results in an estimated bulking factor of 1.31. It is interesting that Listak's study (*36*) deduced that the final caving height occurred approximately 17 ft above the coalbed, which implies that the final bulking factor was 1.34.

With the bulking factor determined, the tangent modulus values can be determined from figure 26 for shape ratios of 0.4 and 0.5. The tangent modulus is determined by interpolating between bulking factor curves for a rock strength of 6,500 psi. Averaging the modulus from both curves yields a tangent modulus of 5,125 psi. This same procedure is used to determine the secant modulus of 2,125 psi from figure 25.

Comparing the moduli values obtained from both methods shows that the second method, using multiple regression analysis, produces lower values. The moduli values found using the second method are based mostly on second-order effects (i.e., shape ratio, rock strength), whereas the first method is based on a first-order effect of the stress level that directly impacts the behavior of the gob.

The bulking factor of the actual gob material is probably dependent upon its position within the gob and the point in time that it is evaluated during the longwall process. For example, immediately after the roof falls, creating the gob, the bulking factor will start to decrease as the gob gradually takes on more load and further compacts. Since the behavior of the in situ gob is so complex, this study assumed that the bulking factor was an average of the volume monitored during the test with the uniaxial loading representing the final compaction of the gob.

Although the second method neatly quantifies factors into the determination of the modulus, the errors of not including other unknown factors and potential first-order effects (i.e., bulking factor gradation, caving height, degree of fracturing of the immediate roof) may only compound the error involved. Consequently, with so many unknown gob behavior parameters that were impossible to factor into the second method, it seems more appropriate to use the first method to conservatively approximate the behavior of gob.

Most valuable to numerical modelers for estimating the gob modulus is the first method based directly on the stress level (fig. 22). These curve equations and ranges can be implemented into the numerical program to model the strain-hardening behavior of the gob and thereby produce more credible results.

CONCLUSIONS AND RECOMMENDATIONS

As table 2 attests, there has been a large range of gob modulus values used in past numerical modeling of longwall panels. From comparing previously determined gob modulus values in tables 1 and 2, it is apparent that the results determined in this study (table 6) were most similar to the in situ tests of caved waste material, somewhat lower than other laboratory test results, and remarkably lower than the estimated modulus values used in the numerical modeling (although it is difficult to compare these values equitably).

The test material used in this study was formulated to simulate the composition and gradation of actual gob material. Behavior of the simulated gob material under uniaxial loading produced a nonlinear stress-strain curve, linear stress-secant-modulus curve, and a second-order polynomial stress-tangent-modulus curve. These correlated well with the theoretical solution curves developed by Ryder (*33*) and Salamon (*34*). Although the results of this study cannot be assumed to duplicate gob moduli of all mines, they do present two approximation methods for determining the gob modulus. The first method is based directly on the stress level, independent of rock type (equations are shown on figure 22), while the second method takes into account second-order effects and is based on the stress level, bulking factor, rock strength, and the shape ratio of the gob (equations are shown in table 11). Because of factors unable to be included with this second method, the first method is recommended to determine the approximate modulus for modeling purposes. It is hoped that the results presented in this report will provide a more accurate and consistent means of estimating the gob modulus, which is essential for longwall numerical modeling.

Caution should be exercised when selecting modulus values, especially if the gradation is unknown. Gradations used in this study are based on photographs from mines in the central Appalachian region. The roof rock in this region is quite competent in strength, which may result in a different gradation than that found in other coalfields or seams. Changing the gradation will more likely affect the bulking factor and, subsequently, the gob modulus. If the gob is composed of a greater proportion of uniformly sized rock pieces, the gob will have more void spaces, higher bulking factor, more deformation, and a lower modulus value.

If additional research work is conducted on the behavior of gob material, the test chamber should be designed to monitor loading at the bottom interface of the gob and statistical analyses should be conducted to evaluate simulated gob material of various gradations, shape ratios, and rock strengths. Also, gob gradations in various regions of the United States should be evaluated using photoanalysis and image enhancement techniques.

REFERENCES

1. Mark, C. Practical Aspects of Longwall Pillar Design. Paper in Proceedings of 10th International Conference on Ground Control in Mining. WV Univ., Morgantown, WV, 1991, pp. 1-13.

2. Zipf, R. K. MULSIM/NL Theoretical and Programmers Manual. BuMines IC 9321, 1992, 52 pp.

3. Rice, G. S. Tests of Strength of Roof Supports Used in Anthracite Mines of Pennsylvania. BuMines B 303, 1929, 44 pp.

4. Peng, S. S. Coal Mine Ground Control. Wiley, 1978, 200 pp.

5. Peng, S. S., K. Matsuki, and W. H. Su. 3-D Structural Analysis of Longwall Panels. Paper in The State of the Art in Rock Mechanics: Proceedings of the 21st U.S. Symposium on Rock Mechanics, compiled by D. A. Summers (Rolla, MO, May 28-30, 1980). Univ. MO, 1980, pp. 44-56.

6. Bowling, A. J. Investigations Into the Deformability of Rockfill. Paper in Proceedings of the Third Australian-New Zealand Conference on Geomechanics (Wellington, N.Z., May 12-16, 1980). N.Z. Inst. Eng., 1980, pp. 1-6.

7. Wardle, L. J., and J. R. Enever. Application of the Displacement Discontinuity Method to the Planning of Coal Mine Layouts. Paper in Proceedings of the 5th International Congress on Rock Mechanics (Melbourne, Aust.). A. A. Balkema, 1983, pp. E61-E69.

8. Smart, B. G. D., and S. M. Haley. Further Development of the Roof Strata Tilt Concept for Pack Design and the Estimation of Stress Development in a Caved Waste. Min. Sci. & Technol., v. 5, 1987, pp. 121-130.

9. Trueman, R. A Finite Element Analysis for the Establishment of Stress Development in a Coal Mine Caved Waste. Min. Sci. & Technol., v. 10, 1990, pp. 247-252.

10. Hsiung, S. M., and S. S. Peng. Chain Pillar Design for U.S. Longwall Panels. Min. Sci. & Technol., v. 2, 1985, pp. 279-305.

11. Kripakov, N. P., L. A. Beckett, D. A. Donato, and J. S. Durr. Computer-Assisted Mine Design Procedures for Longwall Mining. BuMines RI 9172, 1988, 38 pp.

12. Beckett, L. A., and R. S. Madrid. MULSIM/BM—A Structural Analysis Computer Program for Mining Design. BuMines IC 9168, 1988, 302 pp.

13. Hackett, T., and H. Park. Ground Control Analysis of Multi-Sluice Mining for Thick Western Coal Seams. Soc. Min. Eng. AIME preprint 87-39, 1987, 8 pp.

14. Maleki, H. N. Development of Modeling Procedures for Coal Mine Stability Evaluation. Paper in Rock Mechanics Contributions and Challenges: Proceedings of the 31st U.S. Symposium, ed. by W. A. Hustrulid and G. A. Johnson (Denver, CO, June 18-20, 1990). A. A. Balkema, 1990, pp. 85-92.

15. Park, D. W., and V. Gall. Supercomputer Assisted Three-Dimensional Finite Element Analysis of a Longwall Panel. Paper in Rock Mechanics as a Guide for Efficient Utilization of Natural Resources: Proceedings of the 30th U.S. Symposium, ed. by W. Khair (Morgantown, WV, June 19-22, 1989). A. A. Balkema, 1989, pp. 133-140.

16. Su, D. W. Finite Element Modeling of Subsidence Induced by Underground Coal Mining: The Influence of Material Nonlinearity and Shearing Along Existing Planes of Weakness. Paper in Proceedings of 10th International Conference on Ground Control in Mining. WV Univ., Morgantown, WV, 1991, pp. 287-300.

17. Heasley, K. A. An Examination of Energy Calculations Applied to Coal Bump Prediction. Paper in Rock Mechanics as a Multidisciplinary Science: Proceedings of the 32nd U.S. Symposium, ed. by J. Roegiers (Norman, OK, July 10-12, 1992). A. A. Balkema, 1992, pp. 481-490.

18. Marachi, N. D., C. K. Chan, H. B. Seed, and J. M. Duncan. Strength and Deformation Characteristics of Rockfill Materials. Dep. Civ. Eng., Univ. CA—Berkeley, Rep. TE-69-5, Sept. 1969, 139 pp.

19. Becker, E., C. K. Chan, and H. B. Seed. Strength and Deformation Characteristics of Rockfill Materials in Plane Strain and Triaxial Compression Tests. Dep. Civ. Eng., Univ. CA—Berkeley, Rep. TE-72-3, Oct. 1972, 121 pp.

20. Fumagalli, E. Test on Cohesionless Material for Rockfill Dams. J. Soil Mech. and Found. Div., Am. Soc. Civ. Eng., v. 95, No. SM1, Jan. 1969, pp. 313-330.

21. Lowe, J. Shear Strength of Coarse Embankment Dam Materials. Paper in Proceedings of the 8th International Congress on Large Dams (Edinburgh, U.K., May 4-8, 1964). Publ. Com. Int. Grands Barrages, 1964, pp. 745-761.

22. Franklin, J. A., N. H. Maerz, and C. P. Bennett. Rock Mass Characterization Using Photoanalysis. Int. J. Min. and Geol. Eng. (U.K.), v. 6, 1988, pp. 97-112.

23. American Society for Testing and Materials. Standard Method of Making and Curing Concrete Test Specimens in the Laboratory. C192-90a in 1991 Annual Book of ASTM Standards: Volume 4.02, Construction. Philadelphia, PA, 1991, pp. 115-121.

24. Ferm, J. C., and G. C. Smith. A Guide to Cored Rocks in the Pittsburgh Basin. Dep. Geol., Univ. KY, Lexington, KY; Dep. Geol., Univ. SC, Columbia, SC; 1980, 109 pp.

25. Krumbein, W. C., and F. J. Pettijohn. Manual of Sedimentary Petrography. Appleton-Century, 1938, pp. 288-289.

26. Krumbein, W. C., and L. L. Sloss. Stratigraphy and Sedimentation. Freeman, 2d ed., 1963, pp. 99-108.

27. American Society for Testing and Materials. Standard Test Methods for Absorption and Bulk Specific Gravity of Natural Building Stone. C97-90 in 1991 Annual Book of ASTM Standards: Volume 4.08, Soil and Rock; Dimension Stone; Geosynthetics. Philadelphia, PA, 1991, pp. 1-5.

28. Vallejo, L. E., R. A. Welsh, and M. K. Robinson. Correlation Between Unconfined Compressive and Point Load Strengths for Appalachian Rocks. Paper in Rock Mechanics as a Guide for Efficient Utilization of Natural Resources: Proceedings of the 30th U.S. Symposium, ed. by W. Khair (Morgantown, WV, June 19-22, 1989). A. A. Balkema, 1989, pp. 461-468.

29. Peng, S. S. Longwall Mining. Wiley, 1984, 708 pp.

30. Marsal, R. J., L. R. DeArellano, and A. G. Nunez. Plane Strain Testing of Rockfill Materials. Paper in Proceedings of Third Pan-American Conference on Soil Mechanics and Foundation Engineering (Caracas, Venezuela). 1967, pp. 249-271.

31. Athanasiou-Grivas, D., and M. E. Harr. Particle Contacts in Discrete Materials. J. Geotech. Eng. Div., Am. Soc. Civ. Eng., v. 106, No. GT5, May 1980, pp. 559-564.

32. Doornkamp, J. C., and C. A. M. King. Numerical Analysis in Geomorphology—An Introduction. St. Martin's Press (U.K.), 1971, 372 pp.

33. Ryder, J. A., and H. Wagner. 2D Analysis of Backfill as Means of Reducing Energy Release Rates at Depth. Chamber of Mines, S. Afr., Res. Organ., Res. Rep. 47/78, 22 pp.

34. Salamon, M. D. G. Mechanism of Caving in Longwall Coal Mining. Paper in Rock Mechanics Contributions and Challenges: Proceedings of the 31st U.S. Symposium, ed. by W. A. Hustrulid and G. A. Johnson (Denver, CO, June 18-20, 1990). A. A. Balkema, 1990, pp. 161-168.

35. Salamon, M. D. G. (Colorado School of Mines). Private communication, 1991; available upon request from D. M. Pappas, Pittsburgh Res. Cent., BuMines, Pittsburgh, PA.

36. Listak, J. M., J. L. Hill, and J. C. Zelanko. Direct Measurement of Longwall Strata Behavior: A Case Study. BuMines RI 9040, 1986, 19 pp.

APPENDIX.—ADDITIONAL TEST DATA

Tables A-1 through A-3 show printouts of point load test data and estimated rock compressive strengths from a computer spreadsheet program.

Table A-1.—Point load test results used for estimating compressive strength of shale

TEST	AVG WIDTH (in)	(mm)	DEPTH (mm)	FAIL LD (kg/cm2)	P (kN)	De2 (mm2)	De (mm)	Is	F	Is50	
					PERPENDICULAR TO BEDDING						
1	1.1	27.94	21.5	48.5	6.862	764.85	27.66	8.971	0.766	6.873	
2	0.85	21.46	21.5	27.5	3.891	587.54	24.24	6.622	0.722	4.78	
3	0.9	22.86	22	33	4.669	640.34	25.3	7.291	0.736	5.367	
4	1.14	28.96	28	47	6.649	1032.3	32.13	6.441	0.82	5.279	
5	0.65	16.51	14	17	2.405	294.3	17.16	8.172	0.618	5.05	
6	1.76	44.7	19	23	3.254	1081.5	32.89	3.009	0.828	2.492	XL
7	0.55	13.97	10	13	1.839	177.87	13.34	10.34	0.552	5.705	
8	0.85	21.59	11.5	25	3.537	316.13	17.78	11.19	0.628	7.026	XL
9	0.58	14.73	11	17	2.405	206.33	14.36	11.66	0.57	6.65	
10	0.85	21.59	16.5	29	4.103	453.57	21.3	9.046	0.681	6.161	
11	0.55	13.97	11	20	2.83	195.66	13.99	14.46	0.564	8.152	XL
12	0.65	16.51	10	17	2.405	210.21	14.5	11.44	0.573	6.554	
13	1.1	27.94	23	19	2.688	818.21	28.6	3.285	0.778	2.555	XL
14	0.72	18.29	16	23	3.254	372.56	19.3	8.734	0.652	5.691	
15	1.25	31.75	18.5	37	5.235	747.87	27.35	6.999	0.762	5.335	
16	0.9	22.86	12	23	3.254	349.28	18.69	9.316	0.642	5.983	
									AVG	5.785	
							COMPRESSIVE	STRENGTH		10,486 PSI	
					PARALLEL TO BEDDING						
1	0.86	21.84	18.5	11.5	1.627	514.53	22.68	3.162	0.701	2.216	
2	0.96	24.38	17	17	2.405	527.79	22.97	4.557	0.705	3.211	
3	0.71	18.03	16	7.5	1.061	367.39	19.17	2.888	0.65	1.876	
4	0.58	14.73	22	18	2.547	412.66	20.31	6.171	0.667	4.115	
5	0.86	21.84	20	15	2.122	556.25	23.59	3.815	0.713	2.721	
6	0.8	20.32	17	21	2.971	439.83	20.97	6.755	0.676	4.569	XL
7	0.43	10.92	11	9	1.273	152.97	12.37	8.324	0.533	4.439	
8	0.46	11.68	22	14	1.981	327.28	18.09	6.052	0.633	3.83	
9	0.75	19.05	22	7	0.99	533.61	23.1	1.856	0.706	1.311	XL
10	0.55	13.97	13.5	5	0.707	240.13	15.5	2.946	0.59	1.739	
11	0.73	18.54	18	16	2.264	424.95	20.61	5.327	0.671	3.575	
12	0.78	19.81	28	7	0.99	706.31	26.58	1.402	0.752	1.055	XL
13	0.42	10.67	11	11	1.556	149.41	12.22	10.42	0.531	5.526	XL
14	0.45	11.43	11	4	0.566	160.08	12.65	3.535	0.539	1.905	
									AVG	2.962	
							COMPRESSIVE	STRENGTH		5,370 PSI	
									OVERALL AVG	4.374	
					COMPRESSIVE STRENGTH =		4.374 x 145 x 12.5 =			7,930 PSI	

17.4= CONVER FROM PT LD TO COMPR STR.
FOR SHALE
145= CONVER FROM SI TO ENGL UNITS
XL= EXCLUDE FROM AVG. TOP AND BOTTOM
TWO VALUES

P = FAIL LD/ RAM AREA
De2 = (4 x WIDTH x DEPTH)/PI
Is = P/De2
F = (De/50) ^ .45
Is50 = Is x F

Table A-2.—Point load test results used for estimating compressive strength of weak sandstone

TEST	AVG WIDTH (in)	(mm)	DEPTH (mm)	FAIL LD (kg/cm2)	P (kN)	De2 (mm2)	De (mm)	Is	F	Is50	
					PERPENDICULAR TO BEDDING						
1	0.97	24.64	20	9	1.273	627.4	25.05	2.029	0.733	1.487	
2	0.68	17.27	20.5	6	0.849	450.82	21.23	1.883	0.68	1.281	XL
3	1	25.4	15.5	17.5	2.476	501.27	22.39	4.939	0.697	3.441	
4	1.1	27.94	16	12.5	1.768	569.19	23.86	3.107	0.717	2.227	
5	0.8	20.32	14	8.5	1.203	362.21	19.03	3.32	0.647	2.15	
6	1.17	29.72	14.5	12.5	1.768	548.65	23.42	3.223	0.711	2.291	
7	1.15	29.21	18	43	6.083	669.44	25.87	9.087	0.743	6.756	XL
8	1.12	28.45	22	8	1.132	796.86	28.23	1.42	0.773	1.098	XL
9	1.04	26.42	22	18	2.547	739.95	27.2	3.442	0.76	2.617	
10	0.85	21.59	20.5	16	2.264	563.53	23.74	4.017	0.715	2.873	
11	1.5	38.1	14	10.5	1.485	679.15	26.06	2.187	0.746	1.631	
12	0.64	16.26	19	10	1.415	393.26	19.83	3.598	0.66	2.373	
13	0.35	8.89	12	6	0.849	135.83	11.65	6.249	0.519	3.245	
14	0.62	15.75	19.5	21	2.971	390.99	19.77	7.599	0.659	5.005	XL
15	0.78	19.81	13.5	10.5	1.485	340.54	18.45	4.362	0.639	2.785	
									AVG	2.466	
							COMPRESSIVE	STRENGTH		6220 PSI	
					PARALLEL TO BEDDING						
1	0.67	17.02	18.5	7.5	1.061	400.86	20.02	2.647	0.662	1.753	XL
2	0.67	17.02	10	6.5	0.92	216.68	14.72	4.244	0.577	2.448	
3	0.62	15.75	31	13	1.839	621.58	24.93	2.959	0.731	2.163	
4	0.88	22.35	35	13	1.839	996.08	31.56	1.846	0.813	1.501	XL
5	0.86	21.84	15	8	1.132	417.19	20.43	2.713	0.668	1.813	
6	0.8	20.32	17	14.5	2.051	439.83	20.97	4.664	0.676	3.155	
7	0.55	13.97	8.5	9	1.273	151.19	12.3	8.422	0.532	4.48	XL
8	0.52	13.21	19	7.5	1.061	319.52	17.88	3.321	0.629	2.09	
9	0.82	20.83	19.5	12.3	1.74	517.12	22.74	3.365	0.701	2.361	
10	0.34	8.636	20	7.5	1.061	219.91	14.83	4.825	0.579	2.792	
11	0.7	17.78	11.5	8	1.132	260.34	16.14	4.347	0.601	2.613	
12	0.66	16.76	17	13	1.839	362.86	19.05	5.069	0.648	3.283	XL
13	0.82	20.83	14.5	11	1.556	384.53	19.61	4.047	0.656	2.656	
14	0.4	10.16	9	4	0.566	116.43	10.79	4.861	0.502	2.438	
15	0.53	13.46	10	6.5	0.92	171.4	13.09	5.365	0.547	2.936	
									AVG	2.497	
							COMPRESSIVE	STRENGTH		6300 PSI	
									OVERALL AVG	2.483	
						COMPRESSIVE STRENGTH =		2.483 x 145 x 17.4 =		6263 PSI	

17.4= CONVER FROM PT LD TO COMPR STR.
FOR SANDSTONE
145= CONVER FROM SI TO ENGL UNITS
XL= EXCLUDE FROM AVG. TOP AND BOTTOM
TWO VALUES

P = FAIL LD/ RAM AREA
De2 = (4 x WIDTH x DEPTH)/PI
Is = P/De2
F = (De/50) ^ .45
Is50 = Is x F

Table A-3.—Point load test results used for estimating compressive strength of strong sandstone

TEST	AVG WIDTH (in)	WIDTH (mm)	DEPTH (mm)	FAIL LD (kg/cm2)	P (kN)	De2 (mm2)	De (mm)	Is	F	Is50	
					PERPENDICULAR TO BEDDING						
1	0.76	19.3	15	34.5	4.881	368.68	19.2	13.24	0.65	8.606	
2	0.71	17.91	8	24.5	3.466	182.4	13.51	19	0.555	10.54	XL
3	0.68	17.27	11	24	3.395	241.91	15.55	14.04	0.591	8.299	
4	0.86	21.84	31	60	8.489	862.19	29.36	9.845	0.787	7.748	
5	0.77	19.56	32	55	7.781	796.86	28.23	9.765	0.773	7.55	
6	0.35	8.89	10	15.5	2.193	113.19	10.64	19.37	0.498	9.655	XL
7	0.55	13.97	14.5	19	2.688	257.91	16.06	10.42	0.6	6.252	
8	0.81	20.57	15	30	4.244	392.93	19.82	10.8	0.659	7.123	
9	0.56	14.22	13.5	17	2.405	244.49	15.64	9.837	0.593	5.83	
10	0.95	24.13	15	32.5	4.598	460.85	21.47	9.977	0.684	6.82	
11	1.48	37.59	9.5	24	3.395	454.7	21.32	7.467	0.681	5.089	
12	0.7	17.78	15.5	19	2.688	350.89	18.73	7.661	0.643	4.925	XL
13	0.52	13.21	10	20	2.83	168.17	12.97	16.83	0.545	9.167	
14	0.91	23.11	13.5	18.5	2.617	397.3	19.93	6.588	0.661	4.355	XL
									AVG	7.248	
						COMPRESSIVE		STRENGTH		18,287 PSI	
					PARALLEL TO BEDDING						
1	0.86	21.84	17.5	25	3.537	486.72	22.06	7.267	0.692	5.029	
2	0.52	13.21	17	22	3.112	285.89	16.91	10.89	0.614	6.684	
3	0.77	19.56	20	25.5	3.608	498.04	22.32	7.244	0.696	5.039	
4	0.8	20.32	15	20	2.83	388.08	19.7	7.291	0.658	4.795	XL
5	0.58	14.73	22	37	5.235	412.66	20.31	12.68	0.667	8.458	XL
6	0.34	8.636	10.5	11	1.556	115.45	10.74	13.48	0.501	6.748	
7	0.41	10.41	9.5	6.5	0.92	125.97	11.22	7.3	0.511	3.727	XL
8	0.4	10.16	11	11.5	1.627	142.3	11.93	11.43	0.525	6	
9	0.69	17.53	10	18.5	2.617	223.15	14.94	11.73	0.581	6.81	XL
10	0.71	18.03	21	24	3.395	482.19	21.96	7.042	0.691	4.863	
									AVG	5.727	
						COMPRESSIVE		STRENGTH		14,229 PSI	
									OVERALL AVG	6.487	
					COMPRESSIVE STRENGTH =		6.487 x 145 x 17.4 =			16,368 PSI	

17.4= CONVER FROM PT LD TO COMPR STR. FOR SANDSTONE
145= CONVER FROM SI TO ENGL UNITS
XL= EXCLUDE FROM AVG. TOP AND BOTTOM TWO VALUES

P = FAIL LD/ RAM AREA
De2 = (4 x WIDTH x DEPTH)/PI
Is = P/De2
F = (De/50) ^ .45
Is50 = Is x F

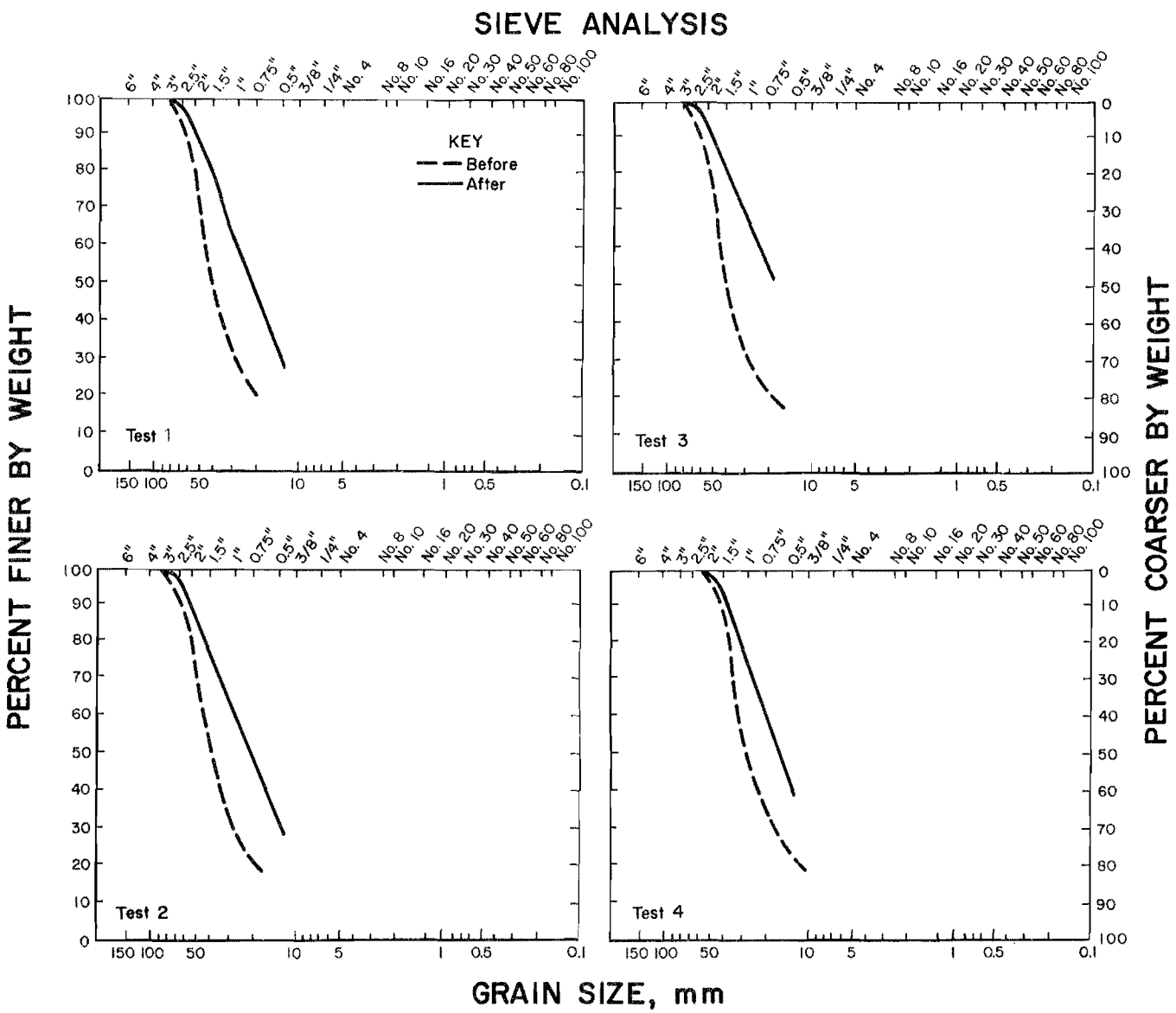

Figure A-1.—Test material gradation curves before and after test.

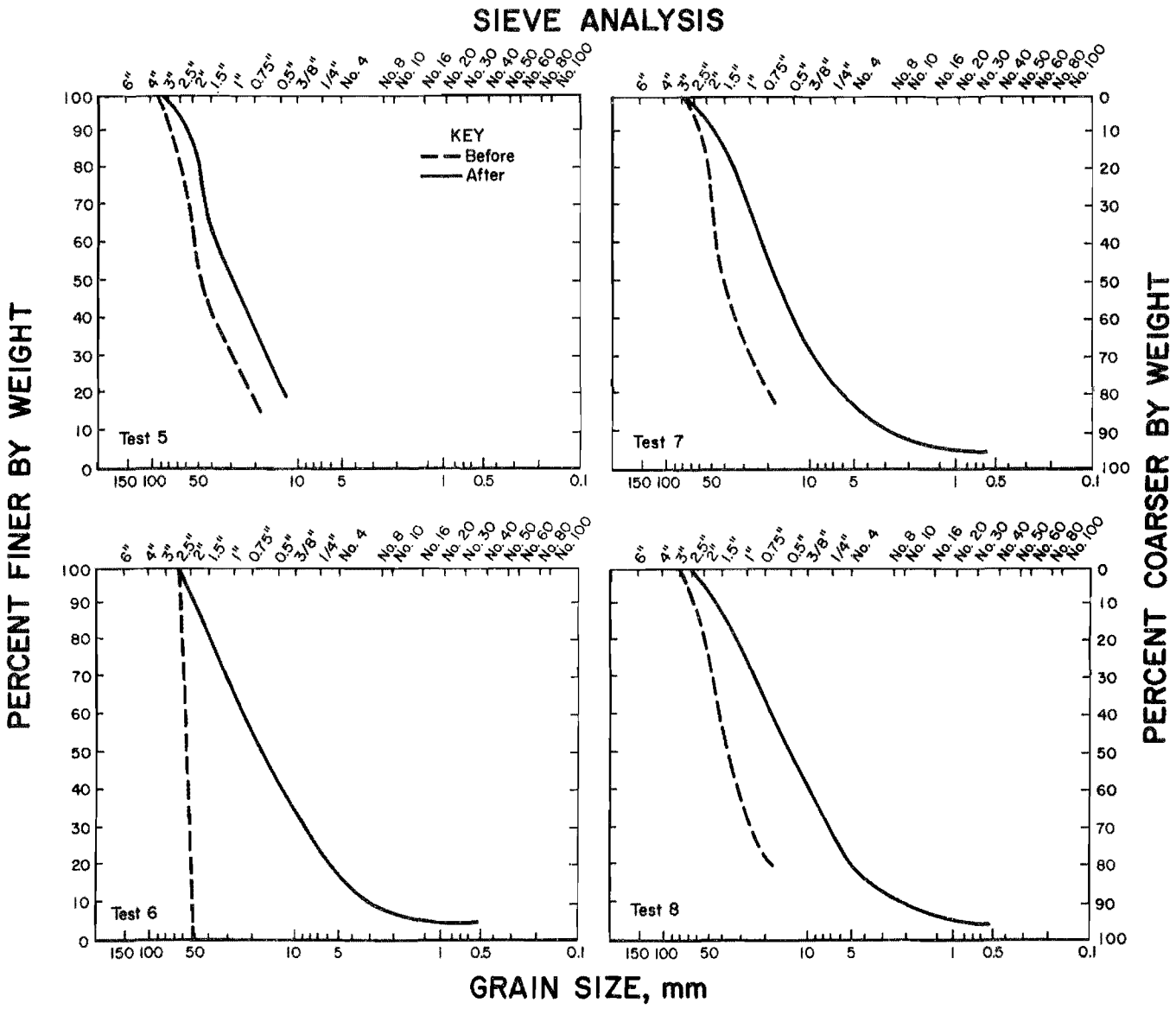

Figure A-1.—Test material gradation curves before and after test—Continued.

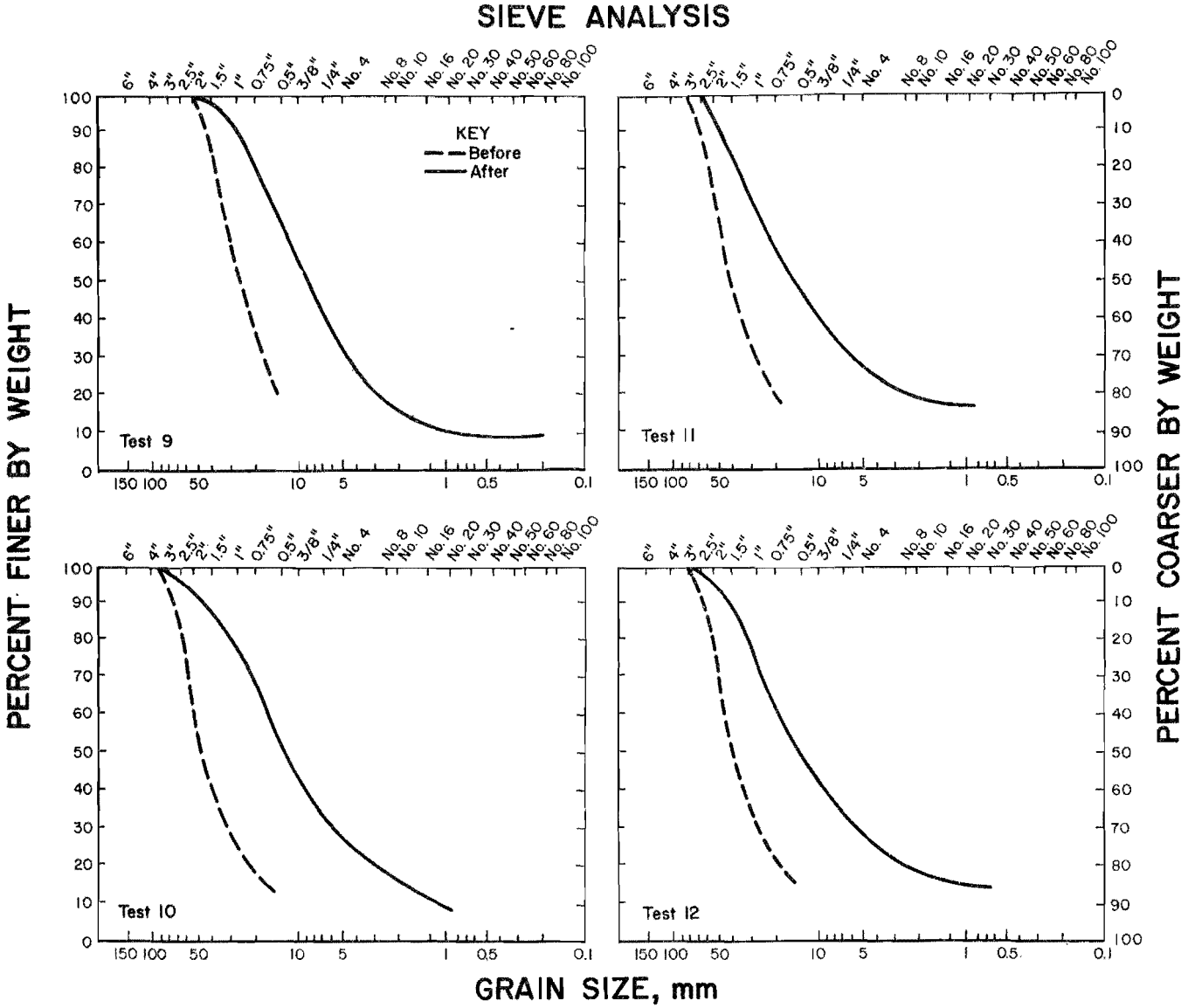

Figure A-1.—Test material gradation curves before and after test—Continued.

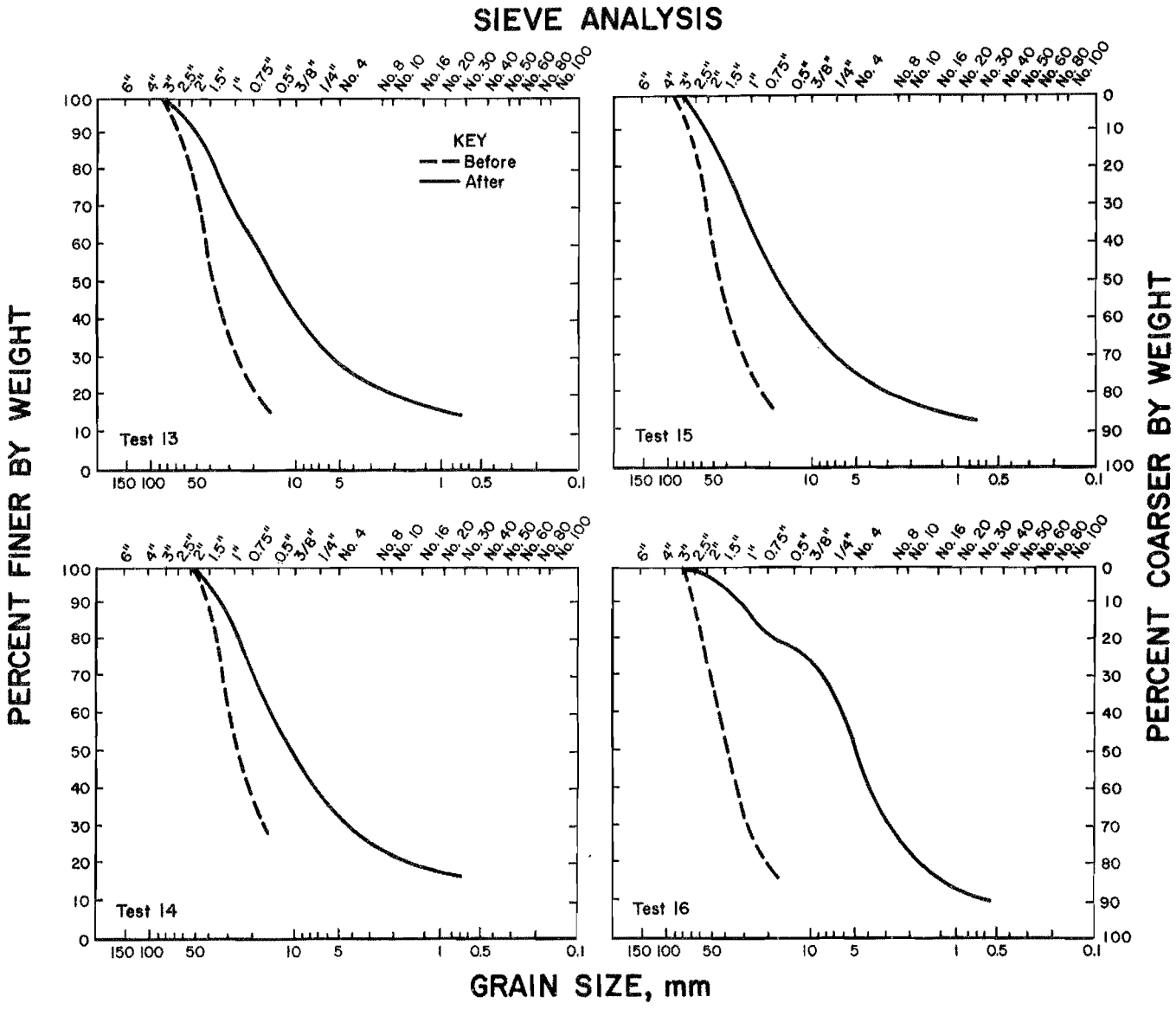

Figure A-1.—Test material gradation curves before and after test—Continued.

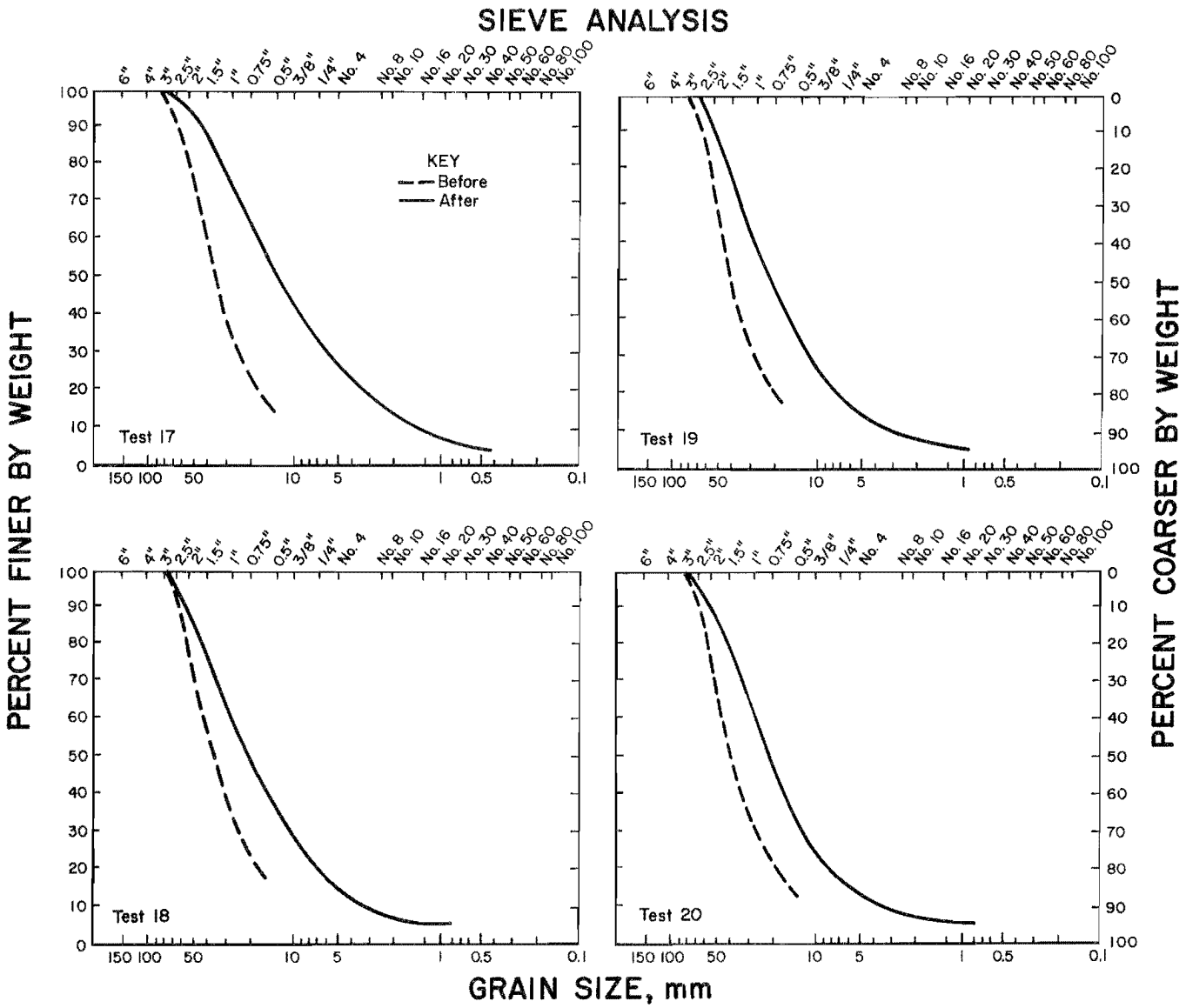

Figure A-1.—Test material gradation curves before and after test—Continued.

INT.BU.OF MINES,PGH.,PA 29734

*U.S.G.P.O.: 1993--709-008/80006